blocks [26]. This method successfully improved the surface wettability and lubrication and decreased the biofouling tendency of PDMS. Although the modification of the PDMS surface with MPC via a chemical reaction is a powerful tool for enhancing the properties of PDMS, the process is complex and it is difficult to modify intricately shaped devices after fabrication. More practical methods have been reported by Sibarani et al., who modified the PDMS surface by a simple treatment method [27], and Seo et al., who modified the PDMS surface by swelling–deswelling methods using ABA-type block copolymers composed of PMPC (A) and PDMS (B) segments [28]. The relative simplicity of these processes renders them more applicable than grafting polymerization and chemical reaction processes. However, the disadvantage of these methods is that low-polarity solvents such as chloroform are used for the surface treatment process because of the low surface energy of PDMS. These solvents induce swelling of PDMS, and consequently, this method is unsuitable for tailor-made devices with dimension-specific designs. On the other hand, the adsorption of poly(ethylene oxide)-*block*-poly(propylene oxide)-*block*-poly(ethylene oxide) and poly(L-lysine)-*graft*-poly(ethylene glycol) (PLL-*g*-PEG) on hydrophobic surfaces in aqueous environments has been reported [29–31]. Lee et al. investigated the adsorption behavior of PLL-*g*-PEG on the PDMS surface by changing the molecular weight of the copolymer and varying the solvent parameters such as pH and salt concentration. They suggested that the large number of hydrophobic groups in the copolymer and the extended conformation of the polymer in aqueous solution are associated with the ease of adsorption of the polymer [31]. For surface modification of biomedical devices, stability of the adsorbed polymer layer under aqueous conditions is essential. In general, proteins can be readily adsorbed from an aqueous medium onto various surfaces. Surface adsorption is normally irreversible owing to conformational changes of the proteins on the surface. Although surface adsorption of protein is a complex process, hydrophobic interaction and electrostatic forces generated at the interface are some of the dominant forces [32]. When proteins approach a surface, the water molecules between surrounding proteins and the surface are removed by an entropic effect. This phenomenon induces a conformational change in the proteins, and the proteins are irreversibly adsorbed on the surface by hydrophobic interaction and electrostatic interaction. We hypothesized that a molecular design similar to the protein structure, with hydrophobic portions and electric charges, should be suitable for the surface treatment of PDMS. PDMS is an elastic material, its surface is hydrophobic, and its surface ζ potential is −44.1 mV [27]. Therefore, we chose 2-ethylhexyl methacrylate (EHMA) and 2-(*N*,*N*-dimethylamino)ethyl methacrylate (DMAEMA) as monomer units of the MPC polymer, with the expectation of hydrophobic interactions and electrostatic attraction forces. The objective of this study was to modify the PDMS surface with the MPC polymer by simple treatment from aqueous solution, thereby negating the swelling effects of low-polarity solvents on PDMS. The influence of the electric charge of the polymer chain and the polymer conformation in aqueous solution on the modification of the PDMS surface is investigated herein by varying the ratio of water and ethanol in the mixture used as the solvent.

2. Experimental

2.1. Materials

MPC was synthesized according to a previously reported method [33]. EHMA, DMAEMA and sodium 1-anilino-8-naphtalene sulfonate (ANS-Na) were purchased from Tokyo Kasei Kogyo (Tokyo, Japan). Liquid PDMS (Silpot 184®) and its curing agent were purchased from Toray-Dow Corning Asia Co. The other reagents and solvents were commercially available in extra-pure grade and used without further purification.

2.2. Synthesis of positively charged amphiphilic polymer

Poly(MPC-*co*-EHMA-*co*-DMAEMA) (PMED) and poly(MPC-*co*-EHMA) (PMEH) were synthesized by a conventional radical polymerization method in ethanol using 2,2′-azobisisobutyronitrile (AIBN) as the radical initiator. The polymerization was carried out at 60 °C. The formed polymer was purified by pouring the reaction mixture into an excess volume of ether/chloroform (8/2, v/v) for precipitation. Furthermore, unreacted MPC was removed by crushing the precipitated polymer and washing with water for 2.0 h. The polymer was collected by filtration and lyophilized. The chemical structure of the polymer was confirmed by ^{1}H NMR in CD_3CD_2OD, the molecular weight of the polymer was evaluated by gel permeation chromatography (GPC, Jasco, Tokyo, Japan) using hexafluoroisopropanol (HFIP) as the eluent, and the retention time was compared with that of the poly(methyl methacrylate) standard. The chemical structure of PMED and PMEH is shown in Fig. 1.

2.3. Fluorescence measurement using ANS-Na

The polarity of the PMED and PMEH solutions prepared in a mixed solvent with various ratios of ethanol and water was evaluated by fluorescence measurements using ANS-Na as a probe. The polymers were first completely dissolved in ethanol, and water was then added in a prescribed ratio. Subsequently, ethanolic ANS solution was added to each sample and the mixture kept in a dark place. The final polymer concentration was 1.0 wt% and the ANS-Na concentration was 1.0×10^{-5} M. The internal polarity of the polymer aggregate was estimated using the maximum wavelength from the fluorescence of ANS-Na (λ_{ex} = 350 nm, measurement range = 420–650 nm).

2.4. Preparation of PDMS

The precursor of PDMS and curing agent were mixed in a 10:1 (v/v) ratio. The mixtures were evenly spread on a dish and were placed under vacuum to remove air bubbles. The curing reaction was performed at 60 °C for 4.0 h.

2.5. Treatment process

PMED and PMEH were dissolved in ethanol and water was added in a given ratio. Ethanolic polymer (PMED and PMEH) solutions containing water at ratios of 0, 20, 50, and 80 v/v% were prepared and are hereafter referred to as PMED-0, 20, 50, and 80 and PMEH-0, 20, 50, and 80, respectively. The final polymer concentration was adjusted to 1.0 wt%. All PDMS substrates were washed with ethanol prior to the treatment process. The plates were dipped 5 times for a few seconds into the PMED solution and then dried in air. This process was repeated twice and the plates were then completely dried under vacuum.

2.6. Surface characterization

The hydrophilicity of the PMED- and PMEH-treated PDMS surfaces was evaluated by measurement of the air and water contact angles using a static contact angle goniometer (CA-W; Kyowa Interface Science Co., Tokyo, Japan). Water contact angles (θ_{water}) were measured under dry conditions and the air contact angles (θ_{air}) were measured in water. The PDMS substrate was cut to fit dimensions of 10 mm × 40 mm × 1.0 mm and 10 mm × 20 mm × 0.70 mm for the respective air and water contact angle measurements.

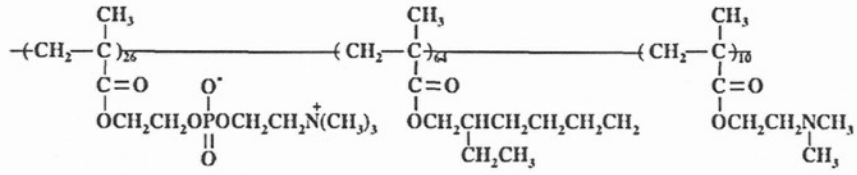

PMED Mw: 2.3 x 10^5

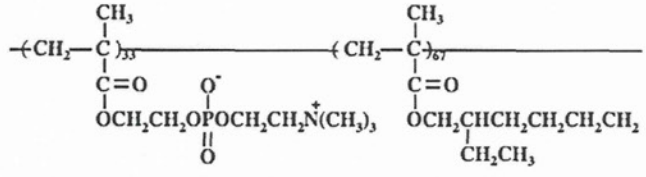

PMEH Mw: 1.2 x 10^5

Fig. 1. Chemical structure of MPC polymers.

The polymer-treated samples were immersed in water for 1 h and were dried under vacuum before contact angle measurements. In the measurement of θ_{water} under dry conditions, water droplets were brought into contact with the modified PDMS surface and θ_{water} was measured within 10 s using photographic images. θ_{air} was measured in water by attaching the samples to a sample holder, which was then transferred into a glass holder filled with purified water. After 5 min, air bubbles were introduced underneath each sample through U-shaped needles and the contact angles were measured using photographic images. Data were collected at 10 positions for each sample. The stability of the polymer layer was evaluated by immersing the samples in water for 1.0, 24, 72, 120, and 168 h. The surface elemental composition was analyzed using X-ray photoelectron spectroscopy (XPS; AXIS-His165 Kratos/Shimadzu, Kyoto, Japan). The photoelectron take-off angle was fixed at 90°. All of the binding energies were referenced to the C_{1s} peak at 285.0 eV and the corresponding peak areas were used to calculate the respective elemental compositions.

2.7. Friction test

The coefficients of dynamic friction between a Co–Cr ball and the surface of the polymer-treated PDMS samples were measured using a surface property tester (Heidon Type32, Shinto Science Co., Tokyo, Japan). The PDMS substrates were prepared in the box (65 mm × 35 mm × 3.0 mm) and were affixed to the stage. The friction tests were performed in purified water at room temperature with load of 0.98 N, for a maximum of 1.0×10^3 cycles.

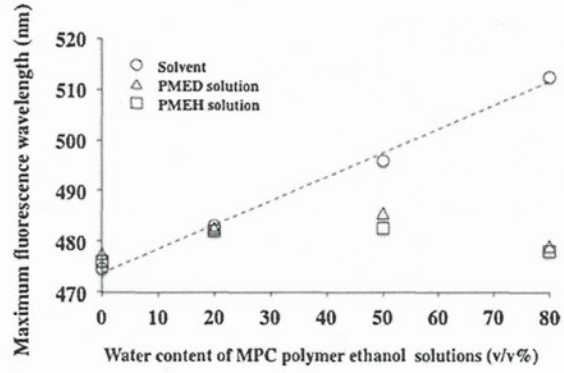

Fig. 2. Peak shifts of ANS-Na fluorescence in MPC polymer solutions.

The scan scale was 20 mm, and the scan speed was 40 mm/s. Three replicate measurements were performed for each sample, and the average values were regarded as the coefficients of dynamic friction.

3. Results and discussion

3.1. Characterization of the solubilized state of PMED in ethanol/water mixture

PMED and PMEH are both soluble in ethanol and do not dissolve in water. In addition, both polymers were soluble in ethanol/water mixtures. The polymer solution was transparent in water con-

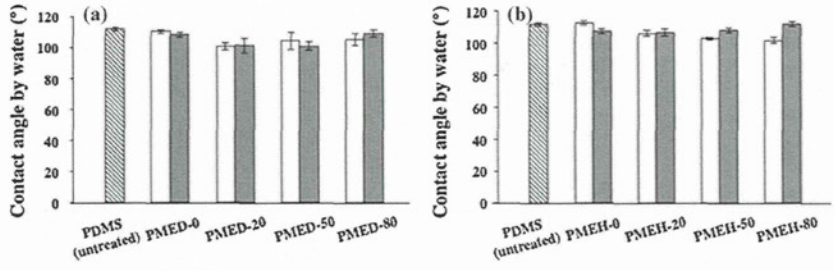

Fig. 3. The contact angles by water on the PDMS surface measured under dry conditions, before and after treatment with PMED (a) and PMEH (b) solution. Open column: just after treatment with the polymer solution. Closed column: after 1.0 h immersion in water.

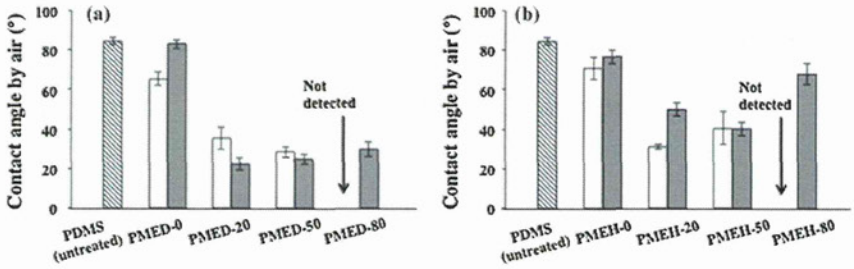

Fig. 4. The contact angles by air on the PDMS surface measured in aqueous solution, before and after coating with PMED (a) and PMEH (b) solution. Open column: just after coating. Closed column: after 1.0 h immersion in water.

tent ranges from 0 v/v% to 80 v/v%. Therefore, the conformation of the polymer changes in ethanol/water mixtures. The solubilized state of PMED and PMEH was evaluated after dissolution in ethanol/water mixtures of various ratios, using ANS-Na as a fluorescence probe. ANS-Na is sensitive to solvent polarity; the fluorescence quantum yield of ANS-Na is enhanced in hydrophobic environments, with a concomitant blue shift of the emission maximum [34]. Fig. 2 shows the emission maximum of ANS-Na in the solvent, PMED solution and PMEH solution. The maximum wavelength of fluorescence (λ_{max}) of ANS-Na in the 80 v/v% aqueous ethanolic solvent was 505 nm. However, the peak was blue-shifted with decreasing content of water. The λ_{max} of ANS-Na was almost the same in both the PMED and PMEH solutions. In the purely ethanolic and 20 v/v% aqueous-ethanolic polymer solutions, the λ_{max} of ANS-Na was almost same as that in the solvent. On the other hand, in the 50 v/v% and 80 v/v% aqueous-ethanolic polymer solutions, the λ_{max} was considerably lower than that in the solvent. The ratio of hydrophilic to hydrophobic units is almost same in both PMED and PMEH. These results indicate that both of the polymers undergo aggregation with increasing water content by hydrophobic interactions. In the 80 v/v% aqueous-ethanolic polymer solution, the polarity of the inside of the polymer aggregate was almost the same as that of ethanol.

3.2. Surface characterization of modified PDMS

The effect of the polymer conformation on the modification of the PDMS surface was investigated after dissolving PMED and PMEH in solvents with different ratios of ethanol to water. Fig. 3 shows the values of contact angles by water (θ_{water}) on the PDMS surface before and after treatment with PMED (a) and PMEH (b). In all samples, high values were obtained for the water contact angles under dry conditions, which were the same as those of untreated PDMS, and the values were not changed after immersion in water for 1 h. The phosphorylcholine group of the MPC polymers is hydrophilic, however, the hydrophobic units of the polymer are enriched at the air interface to decrease the surface free energy [35]. Fig. 4 shows the values of contact angles by air (θ_{air}) on the PDMS surface before and after treatment with PMED (a) and PMEH (b). In contrast to θ_{water} under dry conditions, θ_{air} in water were drastically decreased on the PMED and PMEH-treated surfaces, relative to the untreated surface, with the exception of the surface treated with PMED-0 and PMEH-0 (i.e., purely ethanolic) solutions. θ_{air} could not be measured on the surfaces treated with PMED-80 and PMEH-80, because the air bubble did not attach to the surface. The hydrophilic phosphorylcholine group is exposed in aqueous environments to reduce the interfacial free energy, thus, these results indicate successful treatment of the PDMS surface with PMED-20, 50, and 80 and PMEH-20, 50, and 80. After immersion in water for 1.0 h, the surfaces treated with PMED-20, 50, and 80 maintained their hydrophilicity. However, the contact angles of the surfaces treated with PMEH-20, 50, and 80 were increased after immersion in water for 1.0 h. In particular, the θ_{air} value of the surface treated with PMEH-80 was increased from 0° to 70°. These results indicate that PMEH-20, 50, and 80 were attached to the PDMS surface via weak interactions, and the polymer layer could be easily removed from the PDMS surface during immersion in aqueous solution. The success of the surface treatment with PMED and PMEH was further evaluated by XPS measurement. In the case of the surfaces treated with PMED-20, 50, and 80 and PMEH-20, 50, and 80, ammonium nitrogen and phosphorous peaks were observed at 403 eV and 133 eV, respectively. These atoms were attributed to the MPC unit. On the other hand, there were no peaks in the nitrogen region and phosphorous region for the surfaces treated with PMED-0 and PMEH-0. The results of the XPS and θ_{air} measurements reveal that when ethanol was used as a solvent (in the absence of water), the PDMS surface treatment process was unsuccessful. Fig. 5 shows the relationship between θ_{air} on the PDMS surfaces treated with PMED and PMEH versus the atomic ratio of P/Si of the surface. Contact angle and XPS values after immersion in water for 1.0 h were used for this plot. The atomic ratio of P/Si corresponded to the surface density of the MPC unit; therefore, the density of the phosphorylcholine group could be evaluated on this basis. The contact angle decreased

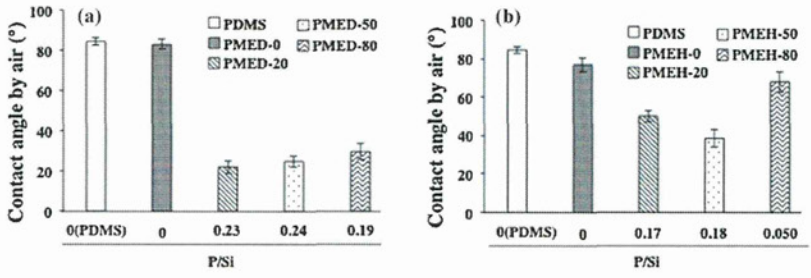

Fig. 5. Atomic ratio of P/Si on the PDMS surface coated with various MPC polymer solutions versus the air contact angles in an aqueous solution.

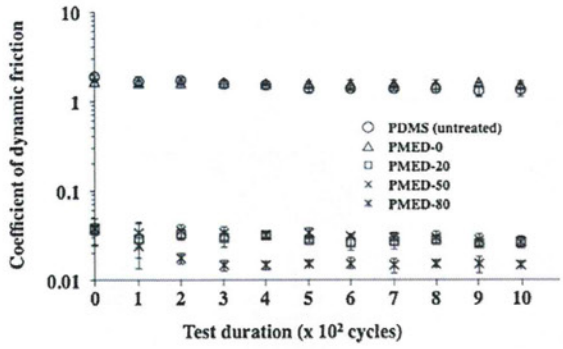

Fig. 6. Time course of the dynamic friction coefficient of the PDMS surface coated with PMED solution.

with an increase in the atomic ratio of P/Si, indicating that the wettability was conferred by the hydrophilic phosphorylcholine group.

3.3. Lubrication property

The lubricity of the surface is important for biomedical devices such as catheters, endoscopes, and artificial joints [19]. The dynamic friction coefficient was used as a parameter for characterizing the lubricity of the PDMS surface treated with PMED in water. Fig. 6 shows the time course of the dynamic friction coefficient between a Co–Cr ball and the surface of PMED-treated PDMS in water. The untreated PDMS surface and PMED-0 treated surface exhibited a very high dynamic friction coefficient of approximately 1.16, consistent with the unsuccessful treatment of the PDMS surface by PMED-0 indicated by the XPS and contact angle measurements. However, after treatment with PMED-20, 50, and 80, the dynamic friction coefficient was dramatically decreased to approximately 0.030, 0.030, and 0.015, respectively. This decrease is attributed to elimination of strong hydrophobic interactions by treatment with hydrophilic PMED. The hydrophilic state ensures the formation of an aqueous lubrication layer and reduces the friction force. The results of the lubrication tests corroborate with the results of the contact angle measurements. Furthermore, the low friction coefficient was maintained during 1.0×10^3 cycles at 0.98 N, demonstrating the stability of the PMED layer formed on the PDMS substrate during the treatment process.

3.4. Stability of MPC polymer on PDMS surface

The stability of the PMED and PMEH layers on the PDMS substrate in aqueous environments was further evaluated by XPS following surface treatment. Fig. 7 shows time course of the elemental ratio of P/Si for the PDMS surfaces treated with PMED (a) and PMEH (b). After immersion in water for 24 h, the atomic ratio of P/Si on the surface treated with PMED-50 and 80 decreased from 0.25 to 0.10. On the other hand, the atomic ratio of P/Si was maintained at 0.25 on the surface treated with PMED-20. All of the treated surfaces maintained an atomic ratio of P/Si of approximately 0.05 over the course of 168 h.

We have previously expounded the relationship between the amount of adsorbed fibrinogen and the surface P/Si ratio [36]. From that study, it is known that the fibrinogen adsorption capacity of the untreated PDMS surface is approximately 1.9 μg/cm^2. The amount of adsorbed fibrinogen was found to decrease with an increase in the atomic ratio of P/Si. In the case of a surface having an atomic ratio of P/Si of 0.035, the amount of fibrinogen adsorbed was significantly reduced to approximately 75% of that observed for the untreated PDMS. On this basis, it is predicted that the surface treated with PMED should exhibit good biofouling resistance after immersion in water for 168 h.

For the surfaces treated with PMEH-20 and 50, the atomic ratio of P/Si decreased from 0.25 to below 0.05 after immersion in water for 24 h, and for the surface treated with PMEH-80, the decrease was even more drastic, moving from approximately 0.15 to 0.05 over an immersion period of only 1.0 h. The P/Si ratio declined to almost 0 after immersion in water for 72 h for all of the treated surfaces. The pK_a of poly(DMAEMA) is about 8.0 [37,38]. In water (pH 5.6), more than 90% of the dimethyl amino groups are protonated. Therefore, PMED is positively charged and was more strongly adsorbed than PMEH; in particular, PMED-20 exhibited the highest stability among all the tested PMED types.

Fig. 8 shows an illustration of the relationship between the solubilized state of the polymer and the adsorption behavior of the polymer on the PDMS substrate. On the basis of the fluorescence measurements using ANS-Na, it was evident that neither PMED nor PMEH could form hydrophobic domains in the purely ethanolic and 20 v/v% aqueous-ethanolic solutions. On the other hand, hydrophobic domains were formed in the 50 v/v% and 80 v/v% aqueous-ethanolic solutions. In purely ethanolic solution, the hydrophobic interaction and electrostatic attraction forces were not operative between the polymer chains and the PDMS surface, therefore, there was no attachment of PMED and PMEH to the surface. In the 20 v/v% aqueous-ethanolic solutions of both polymers, the polymer chains were in the stretched conformation, and were adsorbed on the PDMS surface via hydrophobic interactions. However, the stability of the PMED layer on the surface was much higher than that of the PMEH layer. PMED possesses positive charges in the aqueous solution based on the DMAEMA units, whereas the PDMS surface is negatively charged. Therefore, the difference in the stability of the layers formed by PMED and PMEH suggests that PMED is adsorbed onto the PDMS surface not only by hydrophobic interactions but also by electrostatic attraction forces. In 50 v/v% and 80 v/v% aqueous-ethanolic solutions, PMED and PMEH could form aggregates, with hydrophobic interaction operating as the driving force for aggregation of the hydrophobic units. Because the hydrophobic domain was formed inside the polymer aggregate

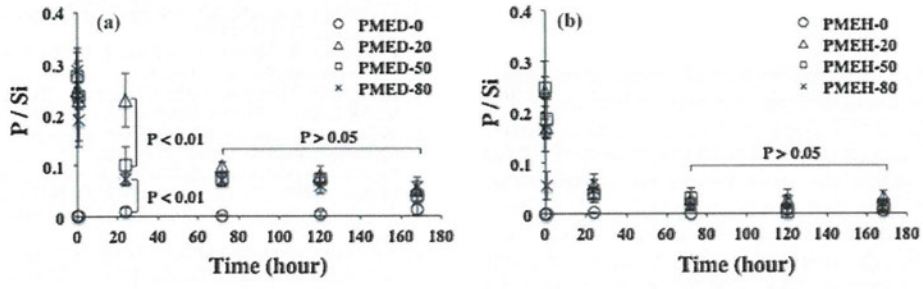

Fig. 7. Time course of the atomic ratio of P/Si on the PDMS surface coated with PMED (a) and PMEH (b) solution.

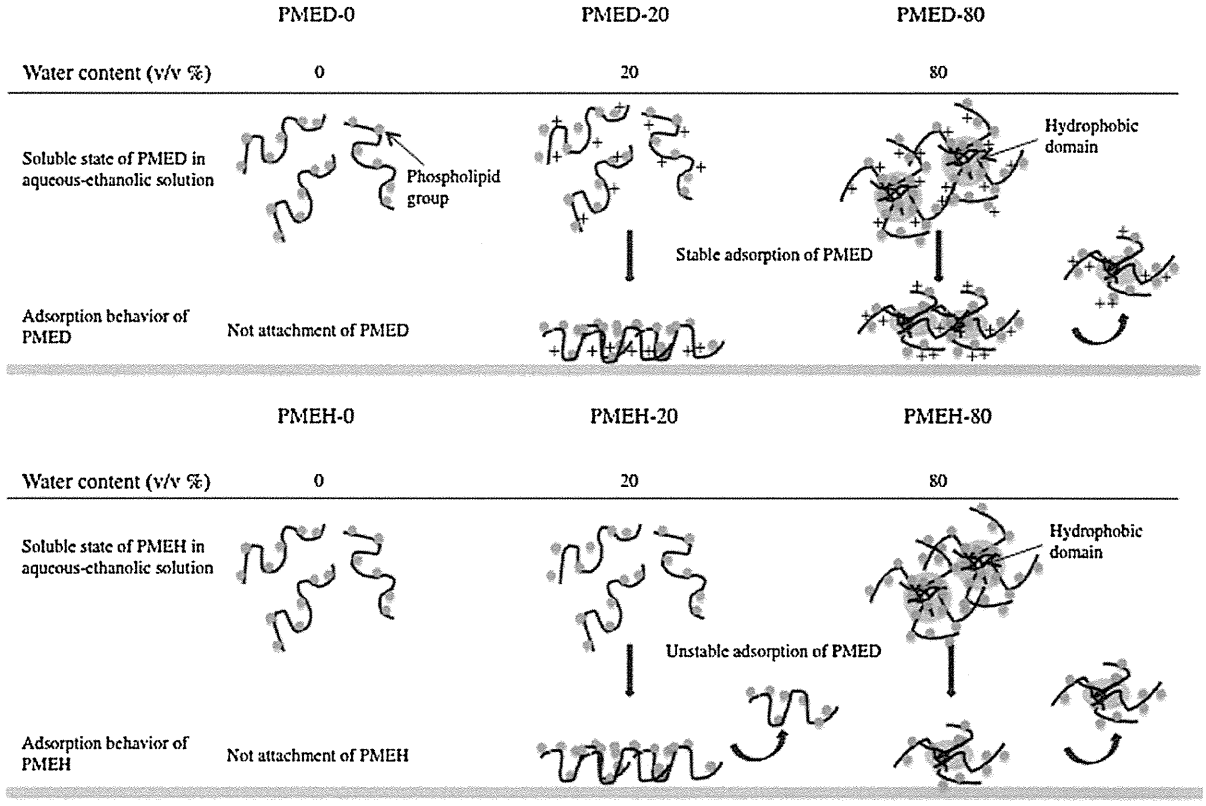

Fig. 8. Schematic illustration of the conformation of PMED and PMEH in aqueous-ethanolic solution and adsorption behavior of PMED and PMEH at PDMS surface.

and the hydrophobic interaction between the polymer chains and the PDMS surface was weakened, PMEH was weakly adsorbed on the PDMS surface. On the other hand, PMED was adsorbed on the PDMS surface primarily via electrostatic forces. Thus, PMED and PMEH may attach to the PDMS surface via either hydrophobic interaction or electrostatic attraction forces. However, both interactions are essential for stable binding between the polymer chains and the PDMS surface. The conformation of a protein is changed after adsorption; the hydrophobic inner surfaces are turned to the outside, and hydrophobic interaction between amino residues and the surface becomes stronger. This is due to the flexible and fragile conformation of proteins. The polymer aggregate is rigid and thermodynamically stable; therefore, the hydrophobic inner region cannot be turned to the outside after adsorption. Thus, the polymer must exist as discrete units in aqueous solution for formation of a stable surface layer, because the hydrophobic interaction between the polymer chains and the surface is weak in the aggregated state.

4. Conclusion

The surface properties of PDMS were readily modified by a simple treatment process using aqueous-ethanolic PMED and PMEH solutions without the need for any pretreatment process. After treatment, the PDMS surface exhibited good water wettability and the dynamic friction coefficient of the surface was decreased by nearly 80% compared with that of the untreated PDMS surface. We demonstrated that the positive charge and hydrophobic moiety were both needed in the polymer for the formation of a stable treatment during treatment of PDMS. Further, we found that the conformation of the polymer in solution influenced the adsorption process. This treatment process is simple and it is possible to apply to various devices made of PDMS after fabrication.

References

[1] M. Chhabra, J.M. Prausnitz, C.J. Radke, Biomaterials 28 (2007) 4331.
[2] M.K. Horne III, K.J. Brokaw, Thromb. Res. 112 (2003) 111.
[3] T.J. Joyce, A. Unsworth, Wear 250 (2001) 199.
[4] J.G. Alauzum, S. Young, R. D'Souza, L. Liu, M.A. Book, H.D. Sheardown, Biomaterials 31 (2010) 3471.
[5] A. Wu, B. Zhao, Z. Dai, J. Qin, B. Lin, Lab Chip 6 (2006) 942.
[6] Y. Yuan, X. Zang, F. Ai, J. Zhou, J. Shen, S. Lin, Polym. Int. 53 (2004) 121.
[7] S. Pintro, P. Alves, C.M. Matos, A.C. Santos, L.R. Rodrigues, J.A. Teixeira, M.H. Gil, Colloids Surf. B: Biointerfaces 81 (2010) 20.
[8] H. Makamba, Y.Y. Hsieh, W.C. Sung, S.H. Chen, Anal. Chem. 77 (2005) 3971.
[9] M. Farrell, S. Beaudoin, Colloids Surf. B: Biointerfaces 81 (2010) 468.
[10] H. Chen, Z. Zhang, Y. Chen, M.A. Brook, H.D. Sheardown, Biomaterials 26 (2005) 2391.
[11] M. Ouyang, C. Yuan, R.J. Muisener, A. Boulares, J.T. Koberstein, Chem. Mater. 12 (2000) 1591.
[12] D. Bodas, C.K. Malek, Microelectr. Eng. 83 (2006) 1277.
[13] M. Morra, E. Occhiello, R. Marola, F. Garbassi, P. Humphrey, D. Johnson, J. Colloid Interface Sci. 137 (1990) 11.
[14] Y. Inoue, T. Nakanishi, K. Ishihara, React. Funct. Polym. 71 (2011) 350.
[15] R. Matsuno, K. Ishihara, NanoToday 6 (2011) 61.
[16] K. Ishihara, N.P. Ziats, B.P. Tierney, N. Nakabayashi, J.M. Anderson, J. Biomed. Mater. Res. 25 (1991) 1397.
[17] K. Ishihara, H. Nomura, T. Mihara, K. Kurita, Y. Iwasaki, N. Nakabayashi, J. Biomed. Mater. Res. 39 (1998) 323.
[18] M. Kyomoto, Y. Iwasaki, T. Moro, T. Konno, F. Miyaji, H. Kawaguchi, Y. Takatori, K. Nakamura, K. Ishihara, Biomaterials 28 (2008) 3121.
[19] M. Kyomoto, T. Moro, K. Saiga, F. Miyaji, H. Kawaguchi, Y. Takatori, K. Nakamura, K. Ishihara, Biomaterials 31 (2010) 658.
[20] S.H. Ye, C.A. Johnson Jr., J.R. Woolley, H. Murata, L.J. Gamble, K. Ishihara, W.R. Wagner, Colloids Surf. B: Biointerfaces 79 (2010) 357.
[21] T. Simizu, T. Goda, N. Minoura, M. Takai, K. Ishihara, Biomaterials 31 (2010) 3274.
[22] T. Moro, Y. Takatori, K. Ishihara, T. Konno, Y. Takigawa, T. Matsushita, U.I. Chung, K. Nakamura, H. Kawaguchi, Nat. Mater. 3 (2004) 829.
[23] T. Moro, H. Kawaguchi, K. Ishihara, M. Kyomoto, T. Karita, H. Ito, K. Nakamura, Y. Takatori, Biomaterials 30 (2009) 2995.

[24] T. Goda, T. Konno, M. Takai, T. Moro, K. Ishihara, Biomaterials 27 (2006) 5151.
[25] T. Goda, R. Matsuno, T. Konno, M. Takai, K. Ishihara, Colloids Surf. B: Biointerfaces 63 (2008) 64.
[26] Y. Iwasaki, M. Takamiya, R. Iwata, S. Yusa, K. Akiyoshi, Colloids Surf. B: Biointerfaces 57 (2007) 226.
[27] J. Sibarani, M. Takai, K. Ishihara, Colloids Surf. B: Biointerfaces 54 (2007) 88.
[28] J.H. Seo, R. Matsuno, T. Konno, M. Takai, K. Ishihara, Biomaterials 29 (2008) 1367.
[29] A. Lee, N.D. Spencer, Tribol. Int. 38 (2005) 922.
[30] S. Lee, R. Iten, M. Muller, N.D. Spencer, Macromolecules 37 (2004) 8349.
[31] S. Lee, N.D. Spencer, Langmuir 24 (2008) 9479.
[32] M. Rabe, D. Verdes, S. Seeger, Adv. Colloid Interface Sci. 162 (2011) 87.
[33] K. Ishihara, T. Ueda, N. Nakabayashi, Polym. J. 22 (1990) 355.
[34] T. Konno, J. Watanabe, K. Ishihara, Biomacromolecules 5 (2004) 342.
[35] K. Futamura, R. Matsuno, T. Konno, M. Takai, K. Ishihara, Langmuir 24 (2008) 10340.
[36] K. Ishihara, B. Ando, M. Takai, Nanobiotechnology 3 (2007) 83.
[37] M.J. Bruining, H.G.T. Blaauwgeers, R. Kuijer, E. Pels, R.M.M.A. Nuijts, L.H. Koole, Biomaterials 21 (2000) 595.
[38] A.M. Funhoff, C.F.V. Nostrum, G.A. Koning, N.M.E.S. Nieuwenbroek, D.J.A. Crommelin, W.E. Hennink, Biomacromolecules 5 (2004) 32.

Biosensors and Bioelectronics 40 (2013) 96–101

Contents lists available at SciVerse ScienceDirect

Biosensors and Bioelectronics

journal homepage: www.elsevier.com/locate/bios

Direct observation of selective protein capturing on molecular imprinting substrates

Kyoko Fukazawa [a], Qiang Li [c], Stefan Seeger [c], Kazuhiko Ishihara [a,b,*]

[a] Department of Materials Engineering, School of Engineering, The University of Tokyo, 7-3-1, Hongo, Bunkyo-ku, Tokyo 113-8656, Japan
[b] Department of Bioengineering, School of Engineering, The University of Tokyo, 7-3-1, Hongo, Bunkyo-ku, Tokyo 113-8656, Japan
[c] Institute of Physical Chemistry, University of Zurich, Winterthurerstrasse 190, CH-8057 Zurich, Switzerland

ARTICLE INFO

Available online 30 June 2012

Keywords:
Label-free detection
Intrinsic fluorescence
Molecular imprinting surface
Phospholipid polymer
Surfactant
Photoreaction

ABSTRACT

A sensing interface for specific protein capture was fabricated using a novel molecular imprinting (MIP) process. Bovine serum albumin (BSA) and ovalbumin (OVA) were imprinted on a quartz substrate with modified alkyl groups, and target protein capture was detected using a deep-UV fluorescence image microscope (UVFLIM). The imprinted protein was immobilized to silica beads (diameter: 15 μm) using a phospholipid polymer containing both active ester groups and silane coupling groups, which were used as protein stamps to prepare the imprinting surface. Protein recognition sites were constructed by integrating sodium dodecyl sulfate (SDS) as the ligand, which was immobilized with a biocompatible photoreactive phospholipid polymer. When BSA solution was added to the BSA-based MIP substrate, strong fluorescence was observed from the tryptophan residue of BSA. In contrast, for the OVA-based MIP substrate and non-MIP substrate, no fluorescence was observed. The surface showed good selectivity of BSA against OVA. The phospholipid polymer layer prevented non-specific protein adsorption, resulting in highly selective protein recognition. Further, when the protein-imprinted substrate was constructed without ligands, neither protein was captured on the substrate. We demonstrated the importance of ligand integration for capturing target proteins at specific positions. UVFLIM can be used to detect biomolecules at the single-molecule level by using intrinsic fluorescence without molecular labeling. Our new protein-imprinted surface used with UVFLIM is a versatile tool for capturing biomolecules.

1. Introduction

Biosensors have been developed for use in biomedical diagnosis, environmental monitoring, food safety, and agriculture. The affinity of target molecules for an interface is a critical factor in biosensor performance (Berney et al., 1997; Ibii et al., 2010; Hall et al., 2011). In many cases, to recognize target molecule selectively, natural recognition biomolecules such as antibodies, enzymes and nucleic acids are installed on the sensing substrate. Although they can capture to the target molecules with strong biological affinity, they are unstable chemically and physically and their initial property is disappeared with time. Therefore, robust sensing substrates are necessary for reliable analysis.

Molecular imprinting (MIP), which involves shape and chemical recognition of target molecules by using synthetic polymer systems, is attracting attention, with artificial receptors being replaced by biomolecules (Fu et al., 2007; Hua et al., 2008; Ye and Mosbach, 2008; Wang et al., 2010; Soares da Silva et al., 2012). In the normal MIP process, the functional monomers and cross-linkers are complexed with imprinted molecules via weak interactions and then polymerized in situ to prepare a matrix. Imprinted molecules are extracted from the matrix to provide capturing sites for target molecules. Many successful studies examining the use of MIP for capturing small organic molecules (e.g., amino acids, peptides, nucleotides, and pharmaceuticals) have been reported (Ansell and Mosbach, 1997; Osawa et al., 2006; Yaqub et al., 2011). However, the use of MIP for protein capture is difficult because of the fragility, complexity, and flexible conformation of proteins. To success of protein MIP, it is important to produce the multiple binding sites with high mobility and the denaturation of target proteins should be suppressed during MIP process including polymerization. Additionally, the matrix surface must inhibit non-specific protein adsorption of the protein to enhance selectivity.

Previously, we proposed an MIP procedure for protein capture based on molecular integration (Fukazawa and Ishihara, 2009). Briefly, silica beads, which form a single layer of imprinted protein, were used for surface MIP. Sodium dodecyl sulfate (SDS), an anionic

* Corresponding author at: Department of Materials Engineering, School of Engineering, The University of Tokyo, 7-3-1, Hongo, Bunkyo-ku, Tokyo 113-8656, Japan. Tel.: +81 3 5841 7124; fax: +81 3 5841 8647.
E-mail address: ishihara@mpc.t.u-tokyo.ac.jp (K. Ishihara).

0956-5663/$ - see front matter © 2012 Elsevier B.V. All rights reserved.
http://dx.doi.org/10.1016/j.bios.2012.06.033

surfactant, interacted with the imprinted protein via electrostatic interactions, and the surfactant was fixed using a water-soluble photoreactive phospholipid polymer. After photoreaction, the imprinted protein was removed together with silica beads to form molecular recognition sites. SDS bound to the protein functioned as both a ligand for capturing target protein and reactive points for the photoreactive polymer. However, complete removal of imprinted proteins from the matrix with silica beads was difficult. Complete removal of imprinted proteins from the surface leads to increased capturing efficiency of target protein. Therefore, we designed a 2-methacryloyloxyethyl phosphorylcholine (MPC) polymer with both active ester groups and triethoxysilane groups to immobilize the imprinted protein on silica beads (Mieda et al., 2012). It is well known that MPC polymers effectively prevent protein adsorption (Ishihara et al., 1991; Ishihara et al., 1998; Murphy et al., 1999). Additionally, biomolecules at the MPC polymer surface can maintain and stabilize protein function (Sakaki et al., 1999; Nishizawa et al., 2008; Goto et al., 2008; Tajima et al., 2011). We expect that imprinted proteins can be removed from the matrix with the silica beads and that denaturation can be suppressed during the MIP process.

Protein MIP approaches include bulk, surface, particle, and epitope imprinting (Kryscio and Peppas, 2012). Among these, the surface MIP approach can be combined with a sensor device (Belmont et al., 2007; Sunayama et al., 2010; Zhou et al., 2011). Imprinted protein can be removed more easily from the substrate surface than with the bulk MIP approach, which involves extraction of imprinted proteins from the matrix after polymerization. Only a small amount of protein is imprinted during surface MIP; therefore, a highly sensitive detection system is necessary for determining the concentration of captured target proteins.

In this study, we fabricated a protein MIP as a sensing interface on quartz glass. Captured proteins were detected using a deep-UV fluorescence imaging microscope (UVFLIM). UVFLIM can be used to detect biomolecules at the single-molecule level by using intrinsic fluorescence without molecular labeling (Li et al., 2004; Li and Seeger, 2006, 2009, 2011). Bovine serum albumin (BSA) and ovalbumin (OVA) were selected as target proteins. The effectiveness of the ligand surfactant and selectivity against BSA and OVA were evaluated.

2. Experimental

2.1. Materials

MPC was synthesized according to a previously reported method (Ishihara et al., 1990). Poly(ethylene glycol) monomethacrylate (Blenmer PE-200) were obtained from NOF Co., Ltd. (Tokyo, Japan). Thionyl chloride and 4-azidobenzoic acid were purchased from Tokyo Chemical Industry Co., Ltd. (Tokyo, Japan). Triethylamine (TEA), 2-hydroxyethyl methacrylate (HEMA), and ligroin were purchased from Kanto Chemical Co., Inc. (Tokyo, Japan). HEMA and TEA were purified by distillation and fractions collected at the boiling points (bp) (70 °C/0.2 kPa and 87 °C, respectively), were used. 3-Methacryloxy propyl trimethoxysilane (MPTS) was purchased from Shin-Etsu Chemical Co., Ltd. (Tokyo, Japan). 2-(Carbomethoxy)ethyltrichlorosilane was purchased from Gelest, Inc. Quartz slide glass ($24 \times 24 \times 0.15$–$0.18\ mm^3$) was purchased from Tosoh Quartz Corp. (Yamagata, Japan). Porous silica beads (average particle diameter: 15 μm; average pore diameter: 7 nm) were obtained from Fuji Silysia Chemical (Tokyo, Japan). Bovine serum albumin (BSA, A-8022), ovalbumin (OVA, A-5503), *n*-butyltrichlorosilane, and *p*-nitrophenylchloroformate were purchased from Sigma-Aldrich (St. Louis, MO, USA). Other reagents and solvents were commercially available in extra-pure grade and used without further purification.

2.2. Synthesis of PMSiN for protein stamp bead preparation

p-Nitrophenyloxycarbonyl polyethyleneglycol methacrylate (MEONP) was synthesized according to a previously reported method (Konno et al., 2004). The chemical structure of MEONP was confirmed using ^1H NMR (α-300, JEOL, Tokyo, Japan) in $CDCl_3$. Poly(MPC-*co*-MPTS-*co*-MEONP) (PMSiN) was synthesized by a conventional radical polymerization method in ethanol using 2,2′-azobisisobutyronitrile (AIBN) as a radical polymerization initiator (Ueda et al., 1992). Desired amounts of MPC, MPTS, and MEONP (monomer molar fractions were 0.70, 0.10, and 0.20, respectively, and total monomer concentration was 0.50 M) and AIBN (5.0 mM) were used for polymerization. Polymerization was carried out at 60 °C for 7.0 h. The formed polymer was purified by pouring the reaction mixture into an excess volume of diethylether/chloroform (80/20 v/v) for precipitation. After precipitation, the PMSiN was dissolved again in ethanol. The solution was evaporated under reduced pressure to remove residual diethyl ether and chloroform. The final concentration of the PMSiN–ethanol solution was adjusted to 5.0 wt% and stored in a freezer. The chemical structure of the PMSiN was confirmed using ^1H NMR (α-300, JEOL, Tokyo, Japan) in CD_3CD_2OD. Molecular weight of the polymers was evaluated using gel permeation chromatography (GPC, Jasco, Tokyo, Japan) in 1,1,1,3,3,3-hexafluoroisopropenol, and retention time was compared with that of the poly(methyl methacrylate) standard (Showa Denko, Tokyo, Japan). The chemical structure of PMSiN is shown in Fig. 1.

2.3. Synthesis of PMPAz for matrix preparation

The synthetic procedure for the photoreactive monomer unit, MPAz, was improved from that reported previously (Fukazawa and Ishihara, 2009). 4-Azidobenzoyl chloride (9.0 g, 50 mmol), synthesized using previously described method, was added to a 300-mL three-necked round-bottomed flask equipped with a dropping funnel, thermometer, and magnetic stirrer, and was dissolved in 80 mL of diethyl ether. After the solution was cooled at −10 °C, HEMA (50 mmol) and TEA (50 mmol) were dissolved in 50 mL of diethyl ether and were added drop-wise to the stirred solution over a period of 1 h. The reaction was carried out for 12 h. After filtering the resulting triethylamine hydrochloride (TEAC), the solvent was evaporated under reduced pressure. The residue was dissolved in diethyl ether to precipitate the residual TEAC, which was then filtered out of the solution. Following addition of diethyl ether, unreacted HEMA was extracted using

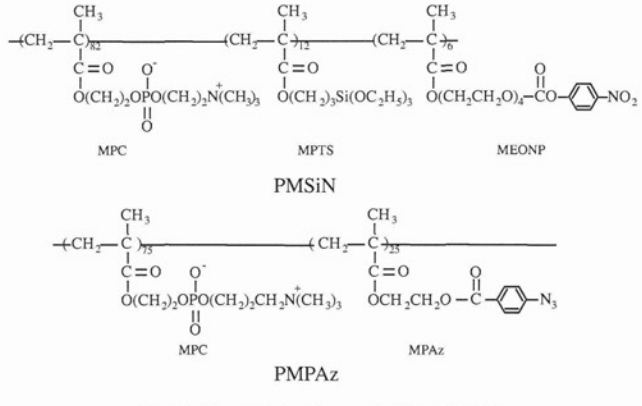

Fig. 1. Chemical structures of MPC polymers.

HCl (10 mM). Diethyl ether solution containing MPAz was dehydrated using anhydrous magnesium sulfate. After filtration to remove magnesium sulfate, the solvent was evaporated under reduced pressure, yielding MPAz in the form of a light yellow oily liquid. Upon freezing, MPAz was converted into a solid. The chemical structure of MPAz was confirmed using ^{1}H NMR in $CDCl_3$ and Fourier-transform infrared spectroscopy (FT-IR) (FT-IR-615, Jasco, Tokyo, Japan). NMR (ppm): 1.95 (d, 3H, α-CH_3), 4.56 (d, 4H, –CH_2CH_2), 5.59 (d, 1H, =CH_2), 6.14 (d, 1H, =CH_2), 7.07 (d, 2H, benzyl), 8.06 (d, 2H, benzyl). IR(cm^{-1}): 3021(p-Ar), 2124 (C–N_3), 1720 (C=O), 1604 (C=C).

Poly(MPC-*co*-MPAz) (PMAz) was synthesized by a conventional radical polymerization method in ethanol using AIBN as a radical polymerization initiator. The desired amounts of MPC and MPAz (monomer molar fractions were 0.70 and 0.30, respectively, and total monomer concentration was 0.50 M) and AIBN (2.5 mM) were used for polymerization. Polymerization was carried out at 60 °C for 3.5 h. The reaction mixture was poured in an excess volume of diethyl ether/chloroform (80/20 v/v) to precipitate the polymer. The precipitated polymer was collected and purified by dialysis against water using a dialysis membrane (cutoff molecular weight=3000). Next, the polymer was freeze-dried. The chemical structure of the PMPAz was confirmed using ^{1}H NMR in CD_3CD_2OD. Molecular weight of the polymers was evaluated using GPC in a mixture of water and methanol (30:70 v/v), and its retention time was compared with that of the poly(ethylene glycol) standard (Tosoh Co., Tokyo, Japan). The chemical structure of PMPAz is shown in Fig. 1.

2.4. Quartz substrate preparation

Alkyl groups were introduced on the quartz substrate to react with PMAz. After cleaning using oxygen plasma (PR500 plasma reactor; Yamato Science, Tokyo, Japan) (300 W, 100 mL/min flow) for 10 min, quartz substrates were placed in toluene solution containing *n*-butyltrichlorosilane (50 mmol) and 2-(carbomethoxy)-ethyltrichlorosilane (50 mmol) for 1 h at room temperature. Next, the quartz substrate was washed by sonication using toluene and methanol.

2.5. Protein stamp preparation

PMSiN was reacted with the surface of silica beads to immobilize imprinted proteins. The 0.50 g of beads were cleaned using oxygen plasma and placed in a 50-mL Eppendorf tube. Subsequently, 25 mL of ethanol solution containing 0.20 wt% PMSiN was added to the tube containing silica beads, and the tube was rotated for 1 h at room temperature. Beads were filtered and transferred to a Teflon® dish for solvent evaporation under atmospheric pressure. Next, the beads were heated at 70 °C for 3 h to react PMSiN with the silica beads. The beads were transferred to a 50-mL Eppendorf tube and washed with ethanol for 1 h to remove unreacted PMSiN, after which they were filtered and dried under a vacuum.

PMSiN–silica beads (10 mg) were placed into Eppendorf tubes. BSA or OVA solution (1.0 mg/mL, pH 7.8 phosphate buffer solution) was added to the each tube. Tubes were rotated at 4 °C for 48 h to immobilize the protein, and the amount of immobilized BSA and OVA on PMSiN–silica beads was determined on the basis of the UV absorbance of the supernatant at 400 nm by using UV/visible spectroscopy (V-560, Jasco Co., Tokyo, Japan); absorbance was based on the *p*-nitrophenoxy anion released during the protein immobilization reaction. After rinsing the beads with pH 7.8 phosphate buffer solution for 10 min, the remaining active ester groups were deactivated using a glycine-containing solution (1.0 mg/mL, pH 7.8 PBS) at 4 °C for 24 h. Beads immobilized with BSA and OVA were rinsed with water for 10 min and the water was removed. This procedure was repeated 3 times. Protein-immobilized beads were used as protein stamp beads.

2.6. Protein imprinting surface preparation

Protein stamp beads were mixed with an aqueous solution containing PMPAz and SDS. The silica bead suspension was placed on the quartz substrate with modified alkyl groups and was dried at 25 °C. Substrates were irradiated using a UV lamp (UV Crosslinker, CL-1000, 254 nm, Funakoshi, Tokyo, Japan) for 1 min (light intensity=80 J/cm^2). Following the photoreaction, protein stamp beads were detached from the substrate via sonication for 10 s. A non-molecular imprinting surface (NMIP) was also prepared using silica beads that had not been subjected to protein immobilization. The morphology of the MIP substrate was observed using a scanning electron microscope (SEM; SM-200, Topcon, Tokyo, Japan). We fabricated MIP on the polyethylene substrate by using same procedure and measured the thickness of the PMPAz layer using an atomic force microscopic (AFM; Nanoscope IIIa, Nihon Veeco, Tokyo, Japan). The thickness was in the range between 100 nm and 400 nm. Furthermore, the BSA structure during MIP process was confirmed using a circular dichroism measurement (CD; J-720W, Jasco, Tokyo, Japan). Before and after photoreaction, the molar ellipticity was $-16{,}576.5^\circ$ cm^2 $dmol^{-1}$ and $-16{,}340.8^\circ$ cm^2 $dmol^{-1}$ at 222 nm, and α-helix content was 41.4% and 40.9%, respectively. In the SDS containing solution (molar ratio of BSA and SDS is 1:5), the molar ellipticity was $-16{,}261.5^\circ$ cm^2 $dmol^{-1}$ at 222 nm, and the α-helix content was 40.1%. The CD spectrum was not changed during photoreaction and in the SDS solutions. The BSA did not have any adverse effect during photoreaction.

2.7. Target protein detection

Capture of target proteins was detected using UVFLIM. UVFLIM consists of a 266-nm UV mode-locked diode-pumped picosecond laser (model GE-100-XHP-FHG, Time-Bandwidth Products, Inc., Switzerland). The laser system provides pulses with a duration of < 10 ps and a repetition rate of 40 MHz; the laser has a maximum power output of 30 mW. The laser power was adjusted by inserting different neutral density filters (Melles Griot). The polarized laser beam was split 50/50 by a beam splitter (Laser Components GmbH, Germany), sending 50% into a high-speed photodiode module (Becker & Hickl GmbH, Berlin, Germany), which is used as deriving the synchronization signal for triggering of the time-correlated single-photon (TCSPC) module. The second beam passed an excitation filter (model 254WB25, Omega Optical) and is directed into the quartz microscope objective (40×, NA=0.80, Partec GmbH, Münster, Germany) by a dichroic beam splitter (model 290DCLP, Omega Optical). Surface scans were performed by moving the sample with a motorized *x,y*-translation stage (Märzhäuser, Wetzlar, Germany). The fluorescence light was collected by the same objective and transmitted through the dichroic mirror. An achromatic lens (LAU-25-200, OFR Inc., 200 mm focal distance) focuses the light onto a pinhole. After the pinhole, the fluorescence emission is detected by a high-speed photomultiplier tube (PMT) detector head (model PMH-100-6, Becker & Hickl GmbH). Two emission band-pass filters (model 330WB60, Omega Optical) -one positioned directly after the lens, and the other positioned directly in front of the detector-discriminate fluorescence against scattered light. The signal pulse of the PMT were fed into a TCSPC PC interface card (SPC-630, Becker & Hickl GmgH, Berlin, Germany) to acquire fluorescence signal. A software using C++ program was developed for synchronization of the scanning motion with the

data acquisition and recording the fluorescence intensity imaging. After adding BSA solution (2×10^{-6} M) and OVA solution (2×10^{-6} M) to the NMIP, the BSA-MIP and the OVA-MIP substrates for 2 h, substrates were rinsed with water and dried under N_2 gas. The substrates were placed onto the *x,y* scanning stage and intrinsic tryptophan emission was recorded after one-photon excitation at 266 nm. The microscopy objective of UVFLIM focuses laser beam to a size of the illumination point about 1 μm in diameter and 3 μm deep. When we take scanning images, we are able to measure all fluorescence generated from MIP protein layer (thickness between 100 nm and 400 nm). The fluorescence intensity of all samples was normalized to same intensity level using MATLAB software.

3. Results and discussion

3.1. Characterization of protein stamps

Silica beads (diameter: 15 μm) were used as MIP stamp substrates for protein imprinting. We designed PMSiN to immobilize the imprinted protein on the surface of silica beads (Fig. 1). PMSiN can react with the MPTS unit on the silica bead surface via a silane coupling reaction, and imprinted proteins can be immobilized using the MEONP unit. MPC units play an important role in immobilized protein stabilization. After the reaction, successful construction of the PMSiN layer was confirmed using XPS analysis. High signal intensities were observed at 402 eV in the N_{1s} region and at 133 eV in the P_{2p} region, which was attributed to the MPC unit. The total amount of MEONP units on the silica beads (6.6×10^{-10} mol/mg) was evaluated using UV spectroscopy after complete hydrolysis of the *p*-nitrophenyloxycarbonyl units in 0.20 M NaOH aqueous solution. The active ester group is labile to the primary amino group of the biomolecules, and a carbamate linkage is produced after bioconjugation (Watanabe and Ishihara, 2006). The amounts of immobilized BSA and OVA were 3.3×10^{-10} mol and 3.2×10^{-10} mol, respectively. Approximately 50% of the active ester group was used to immobilize the proteins, and the remaining active groups were deactivated through reaction with glycine. Protein-immobilized silica beads were used as protein stamps for preparing the MIP surface.

3.2. Characterization of protein MIP substrate

The process for preparing the protein MIP substrate is summarized in Fig. 2. The conformation of proteins is flexible and fragile. Therefore, the ligand should be arranged in a suitable position against the imprinted protein to construct the protein recognition site. It is well known that the surfactant can bind to protein via hydrophobic and electrostatic interactions (Mackie and Wilde, 2005; Sonesson et al., 2008). We employed SDS, an anionic surfactant, as a ligand for specific binding of BSA and OVA. At the lowest concentration of 0.10 mM SDS, 6 SDS molecules were bound per BSA without causing denaturation (Turro et al., 1995; Vasilescu and Angelescu, 1999). In this study, an SDS molecule number that was 5 times larger than the molecules of the immobilized imprinted protein was applied. As a control, the MIP process was carried out without SDS. Other important aspect of protein MIP is suppressing non-specific protein adsorption to the region outside the recognition site. We designed a photoreactive water-soluble polymer, PMPAz (Fig. 1), to prepare the matrix. PMPAz possesses both phosphorylcholine groups and azido groups. Polymers with phosphorylcholine groups effectively suppress nonspecific protein adsorption and cell adhesion due to the nature of the phosphorylcholine groups (Marra et al., 1997; Lu et al., 2001; Inoue and Ishihara, 2010). Azide groups decompose due to UV irradiation, forming nitrene groups, which generate highly reactive radicals. These radicals can attack alkyl groups, which were introduced to the surface and SDS. Thus, the matrix, which exhibits resistance to protein adsorption, was prepared after photoreaction. Ligands bound to the target protein were fixed using PMPAz. After the photoreaction, protein stamps were physically removed from the aqueous medium. The morphology of the quartz substrate was observed using SEM (Fig. 3). Silica beads produced 7-μm dimple-shaped patterns. This indicates that PMPAz reacted with alkyl groups on the quartz substrate to form a thick layer that embedded some of the silica beads.

3.3. Selective capturing of target proteins

It is important to remove imprinted molecules from the matrix after polymerization because target protein capture depends on this removal. The fluorescence based on tryptophan (Trp) residue

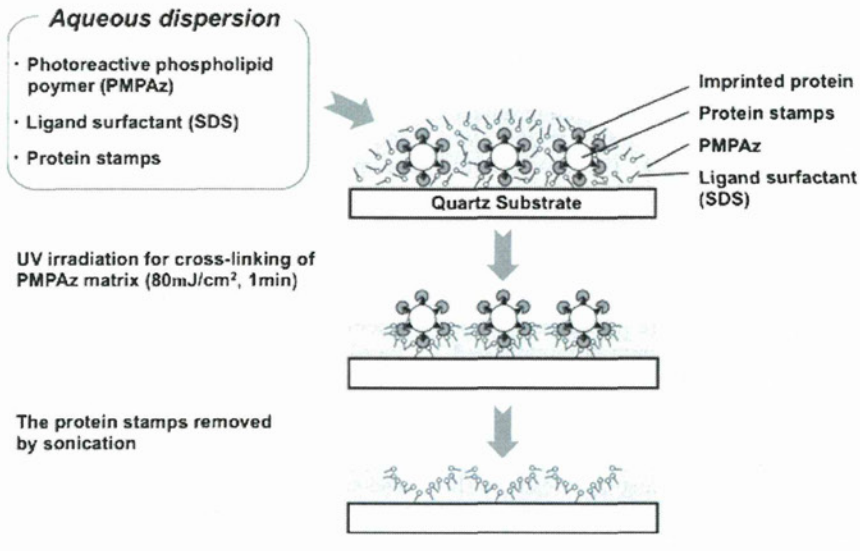

Fig. 2. Procedure for imprinting substrate using molecular integration.

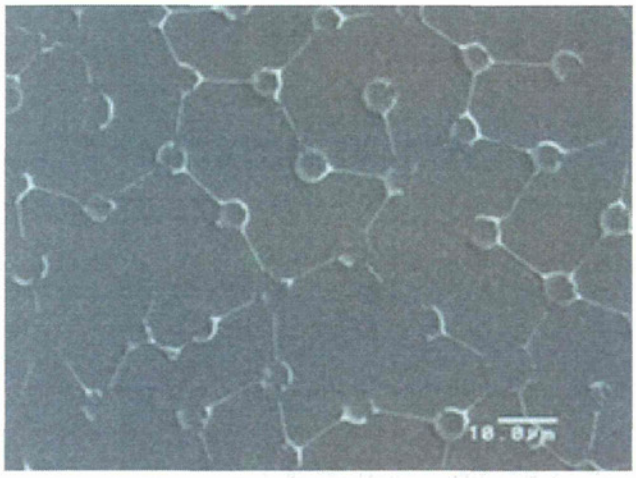

Fig. 3. SEM observation of substrate removing silica beads after photoreaction of PMPAz.

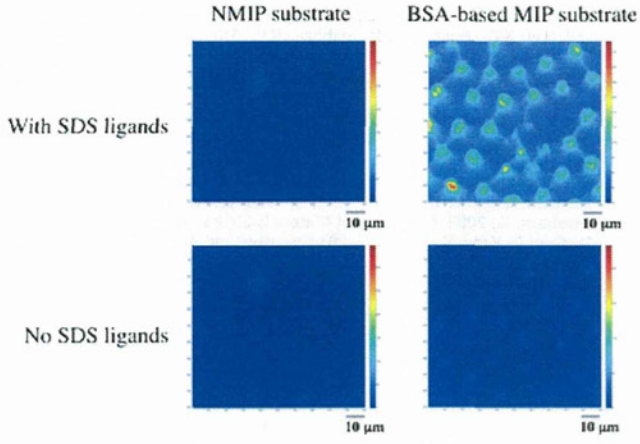

Fig. 4. Fluorescence intensity images by UVFILM after contact with BSA solution to NMIP and BSA-based MIP.

of protein was observed by UVFLIM. Before target protein addition, substrate fluorescence was not observed, indicating that the imprinted protein had been completely removed from the matrix after photoreaction. Fluorescence intensity after addition of the BSA solution to NMIP and BSA-based MIP with or without ligand is shown in Fig. 4. No fluorescence was observed for the NMIP substrates with or without the SDS ligand. Thus, BSA was not captured on these substrates. Additionally, non-specific protein adsorption was suppressed on the PMPAz surface. We observed a strong, dimple-shaped fluorescence pattern on the BSA based-MIP substrate with SDS ligand, and no fluorescence was observed on the BSA based-MIP substrate without ligand. SEM images shown in Fig. 3 were compared with dimple-shaped fluorescent regions, corresponding to the region of protein stamp contact. The target protein, BSA, was captured on the region where BSA was imprinted. We prepared molecular recognition sites on the non-specific protein adsorption surface using this MIP process. The arrangement of SDS ligands against the imprinted protein is important for capturing target proteins because fluorescence was not observed on the substrate.

Both BSA-based MIP and OVA-based MIP substrates were prepared to confirm selective capturing. UVFILM results are shown in Fig. 5. Molecular parameters of BSA and OVA are summarized in Table 1. These molecules possess a different number of aromatic

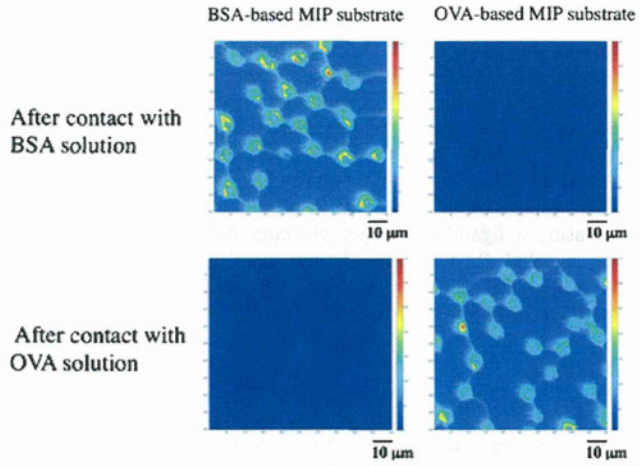

Fig. 5. Fluorescence intensity images by UVFILM after contact with BSA or OVA solution to the BSA-based MIP substrate and OVA-based MIP substrate.

Table 1
Chemical parameters of BSA and OVA.

Protein	Mw (kDa)	pI	Number of amino acid residue in molecule	Aromatic amino acid residues		
				Trp	Tyr	Phe
BSA	69.3	5.82	607	3	21	30
OVA	42.9	5.19	386	3	10	20

amino acid residues, including Trp, tyrosine (Tyr), and phenylalanine (Phe), which contribute to intrinsic fluorescence. However, the intrinsic fluorescence of Tyr is approximately 100 times weaker than that of Trp due to a low extinction coefficient, while the fluorescence emission of Phe is negligible due to a low extinction coefficient and low quantum efficiency. Additionally, transmission of Tyr and Phe fluorescence through our emission filter set is very low due to the blue-shifted emission maximum relative to Trp. Therefore, the intrinsic fluorescence of BSA and OVA was dominated by Trp residues. We can consider fluorescent intensity to represent the degree of adsorption because both BSA and OVA have the same number of Trp residues in 1 molecule. After contact with BSA in BSA-based MIP and OVA-based MIP, we observed strong fluorescence only on the BSA-based MIP substrate. In contrast, after contact with OVA, we observed strong fluorescence only on the OVA-based MIP substrate. Selective capturing against target proteins was observed for the protein MIP substrate. Equal numbers of SDS molecules as a ligand was used, and BSA and OVA have nearly the same isoelectric point. These results indicate that protein capture was not derived from a simple electrostatic interaction between proteins and SDS ligands. A suitable arrangement and density of SDS ligands is important for selective capturing on a substrate. UVFILM does not require molecular labeling of the protein and is sufficiently sensitive to detect low protein levels. Molecular labeling is perhaps disturbed the capturing the target proteins due to change in the chemical and structural nature of the proteins. Here, we showed that UVFILM is a powerful tool for detecting protein capturing on an MIP substrate.

4. Conclusion

Protein recognition sites were artificially constructed on a quartz substrate using the MIP process. Target protein capture

was detected by label-free detection using deep-UVFILM. We demonstrated that the binding sites of target proteins, BSA or OVA, were successfully constructed by integration of SDS molecules by applying 2 types of MPC polymers. MPC polymers provided resistance to non-specific protein adsorption and specificity to the MIP portions. The MIP surface exhibited good selectivity between BSA and OVA based on corresponding MIP proteins, despite having similar isoelectric points. The importance and effectiveness of integrating a ligand for target proteins with a suitable position were revealed. On the basis of these results, we suggest that our new protein MIP surface used in combination with UVFLIM is a versatile system for sensing biomolecules.

References

Ansell, R.J., Mosbach, K., 1997. Journal of Chromatography A 787, 55–66.
Belmont, A.S., Jaeger, S., Knopp, D., Niessner, R., Gauglitz, G., Haupt, K., 2007. Biosensors and Bioelectronics 22, 3267–3272.
Berney, H., Roseingrave, P., Aldermen, J., Lane, W., Collins, J.K., 1997. Sensors and Actuators B 44, 341–349.
Fu, G., Zhao, J., Yu, H., Liu, Li., He, B., 2007. Reactive and Functional Polymers 67, 442–450.
Fukazawa, K., Ishihara, K., 2009. Biosensors and Bioelectronics 25, 609–614.
Goto, Y., Matsuno, R., Konno, T., Takai, M., Ishihara, K., 2008. Macromolecules 9, 828–833.
Hall, W.P., Ngatia, S.N., Van Duyne, R.P., 2011. Journal of Physical Chemistry C 115, 1410–1414.
Hua, Z., Chen, Z., Li, Y., Zhao, M., 2008. Langmuir 24, 5773–5780.
Ibii, T., Kaieda, M., Hatakeyama, S., Shiotsuka, H., Watanabe, H., Umetsu, M., Kumagai, I., Imamura, T., 2010. Analytical Chemistry 82, 4229–4235.
Inoue, Y., Ishihara, K., 2010. Colloids and Surfaces B: Biointerfaces 81, 350–357.
Ishihara, K., Ueda, T., Nakabayashi, N., 1990. Polymer Journal 22, 355–360.
Ishihara, K., Ziats, N.P., Tierney, B.P., Nakabayashi, N., Anderson, James M., 1991. Journal of Biomedical Materials Research 25, 1397–1407.
Ishihara, K., Nomura, H., Mihara, T., Kurita, K., Iwasaki, Y., Nakabayashi, N., 1998. Journal of biomedical materials research 39, 323–330.
Konno, T., Watanabe, J., Ishihara, K., 2004. Biomacromolecules 5, 342–347.
Kryscio, D.R., Peppas, N.A., 2012. Acta Biomaterialia 8, 461–473.
Li, Q., Ruckstuhl, T., Seeger, S., 2004. Journal of Physical Chemistry B 108, 8324–8329.
Li, Q., Seeger, S., 2006. Analytical Chemistry 78, 2732–2737.
Li, Q., Seeger, S., 2009. Sensors and Actuators B 139, 118–124.
Li, Q., Seeger, S., 2011. Journal of Physical Chemistry B 115, 13643–13649.
Lu, J.R., Murphy, E.F., Su, T.J., Lewis, A.L., Stratford, P.W., Satija, S.K., 2001. Langmuir 17, 3382–3389.
Mackie, A., Wilde, P., 2005. Advances in Colloid and Interface Science 117, 3–13.
Marra, K.G., Winger, T.M., Hanson, S.R., Chaikof, E.L., 1997. Macromolecules 30, 6483–6488.
Mieda, S., Amemiya, Y., Kihara, T., Okada, T., Sato, T., Fukazawa, K., Ishihara, K., Nakamura, N., Miyake, J., Nakamura, C., 2012. Biosensors and bioelectronics 31, 323–329.
Murphy, E.P., Lu, J.R., Brewer, J., Russell, J., Penfold, J., 1999. Langmuir 15, 1313–1322.
Nishizawa, N., Konno, T., Takai, M., Ishihara, K., 2008. Macromolecules 9, 403–407.
Osawa, T., Shirasaka, K., Matsui, T., Yoshihara, S., Akiyama, T., Hishiya, T., Asanuma, H., Komiyama, M., 2006. Macromolecules 39, 2460–2466.
Sakaki, S., Nakabayashi, N., Ishihara, K., 1999. Journal of Biomedical Materials Research 47, 523–528.
Soares da Silva, M., Viveiros, R., Aguiar-Ricardo, A., Bonifacio, V., Casimiro, T., 2012. RSC Advances http://dx.doi.org/10.1039/c2ra20426f.
Sonesson, A.W., Blom, H., Hassler, K., Elofsson, U.M., Callisen, T.H., Widengren, J., Brismar, H., 2008. Journal of Colloid and Interface Science 317, 449–457.
Sunayama, H., Ooya, T., Takeuchi, T., 2010. Biosensors and bioelectronics 26, 458–462.
Tajima, N., Takai, M., Ishihara, K., 2011. Analytical Chemistry 83, 1969–1976.
Turro, N.J., Lei, X.G., Ananthapadmanabhan, K.P., Aronson, M., 1995. Langmuir, 2525–2533.
Ueda, T., Oshida, H., Kurita, K., Ishihara, K., Nakabayashi, N., 1992. Polymer Journal 24, 1259–1269.
Vasilescu, M., Angelescu, D., 1999. Langmuir 15, 2635–2643.
Wang, Y., Zhang, Z., Jain, V., Yi, J., Mueller, S., Sokolov, J., Liu, Z., Levon, K., Rigas, B., Rafailovich, M.H., 2010. Sensors and Actuators B 146, 381–387.
Watanabe, J., Ishihara, K., 2006. Biomacromolecules 7, 171–175.
Yaqub, S., Latif, U., Dickert, F.L., 2011. Sensors and Actuators B 160, 227–233.
Ye, L., Mosbach, K., 2008. Chemistry of Materials 20, 859–868.
Zhou, D., Guo, T., Yang, Y., Zhang, A., 2011. Sensors and Actuators B 153, 96–102.

Acta Biomaterialia 8 (2012) 860–865

Contents lists available at SciVerse ScienceDirect

Acta Biomaterialia

journal homepage: www.elsevier.com/locate/actabiomat

Electrically polarized micro-arc oxidized TiO_2 coatings with enhanced surface hydrophilicity

Chufan Ma [a,b], Akiko Nagai [a,*], Yuko Yamazaki [a,c], Takeshi Toyama [c], Yusuke Tsutsumi [d], Takao Hanawa [d], Wei Wang [a], Kimihiro Yamashita [a]

[a] Department of Inorganic Materials, Institute of Biomaterials and Bioengineering, Tokyo Medical and Dental University, 2-3-10 Kanda-Surugadai, Chiyoda-ku, Tokyo 101-0062, Japan
[b] Department of Prosthodontics, School of Stomatology, Fourth Military Medical University, 145, Changlexi Road, Xi'an 710032, People's Republic of China
[c] Department of Materials and Applied Chemistry, College of Science and Technology, Nihon University, 1-8-14 Kanda-Surugadai, Chiyoda-ku, Tokyo 101-8308, Japan
[d] Department of Metals, Institute of Biomaterials and Bioengineering, Tokyo Medical and Dental University, 2-3-10 Kanda-Surugadai, Chiyoda-ku, Tokyo 101-0062, Japan

ARTICLE INFO

Article history:
Received 29 March 2011
Received in revised form 9 August 2011
Accepted 20 September 2011
Available online 24 September 2011

Keywords:
TiO_2 coatings
Micro-arc oxidation
Electric polarization
Hydrophylicity
Oxygen vacancy

ABSTRACT

The use of micro-arc oxidation titania (MAO TiO_2) coatings to modify titanium surfaces improves the biocompatibility of implant surfaces. To obtain hydrophilic MAO TiO_2 coating surfaces electric polarization, which induces surface electric fields in the materials and produces surface charges, was performed in this study. Electric polarization of the MAO TiO_2 coatings was confirmed by measuring the thermally stimulated depolarization current. After electric polarization treatment the MAO TiO_2 coatings did not exhibit any obvious changes in surface roughness, morphology, or phase components. X-ray photoelectron spectroscopy results indicated that electric polarization resulted in oxidation of the cathodic-faced surfaces and reduction of the anodic-faced surfaces. This result suggests that the existence of a concentration gradient of oxide ions/oxygen vacancies produced the stored space charge in the coatings. Reduction of the deionized water contact angle on the polarized MAO TiO_2 surfaces was maintained for longer periods compared with the non-polarized surface. Our study demonstrated that metastable electric fields across the MAO TiO_2 coating produced by electric polarization made it durably wettable by reducing the interfacial surface tension between the material and water.

1. Introduction

Titanium is one of the most widely used biomaterials for dental and orthopedic implants [1,2]. The surface oxide layer is considered an important factor in favorable interactions between tissues and implants [3]. A number of physical and chemical TiO_2 coating methods have been proposed to improve the biocompatibility of implant surfaces [4]. Among them, micro-arc oxidation (MAO), an electrochemical procedure for modifying Ti surfaces, has attracted a great deal of attention [5–7]. The MAO TiO_2 coating is both porous and firmly adheres to the substrate, and both properties are beneficial to the biological performance of the implants. Another advantage of this MAO process is the possibility of incorporating Ca and P ions into the surface coating, by controlling the composition and concentration of the electrolyte, as previous studies have shown that Ca and P phases are beneficial to the bioactivity of the specimens [8,9]. Bioactivity is the ability to communicate with the living body directly. Moreover, this process is well suited to modifying a number of metal substrates with complex geometries, producing an effective chemical barrier against the release of metal ions from the substrate, and can enhance the corrosion resistance of titanium alloys. In the last decade many studies on the biological response to titanium implants have demonstrated that the MAO process constitutes one of the most effective methods of modifying the implant surface [10–12].

Our previous studies showed that electric polarization can be utilized to induce surface electric fields under a d.c. field in bioceramics such as hydroxyapatite (HAp), β-tricalcium phosphate, carbonated hydroxyapatite and bioglasses [13–16]. Surface electric fields in polarized HAp have been experimentally demonstrated in vitro to affect the interfaces between charged surfaces and ions, proteins and cultured cells [17–20]. In vivo surface electric fields also have a remarkable ability to enhance new bone formation on various polarized HAp geometries [21,22]. Moreover, the surface wettability of HAp can be improved by a inducing surface charge via polarization [19,20].

Wettability is an important property of biomaterials because cell adhesion, spreading and differentiation are generally better on hydrophilic surfaces [23,24]. Untreated MAO TiO_2 is known to have a hydrophobic surface. Many studies have reported that MAO TiO_2 surfaces can be made hydrophilic in ambient air by thermal

* Corresponding author. Tel.: +81 352808017; fax: +81 352808015.
E-mail address: nag-bcr@tmd.ac.jp (A. Nagai).

1742-7061/$ - see front matter © 2011 Acta Materialia Inc. Published by Elsevier Ltd. All rights reserved.
doi:10.1016/j.actbio.2011.09.021

annealing, chemical treatment, or UV illumination [8,25,26], however, the hydrophilic MAO TiO_2 becomes hydrophobic over time.

This study investigates the possibility of using electric polarization to make MAO TiO_2 coatings durably wettable. The effects of electric polarization on the microstructure and surface characteristics of the coating were also analyzed.

2. Materials and methods

Titanium discs (ϕ 10 × 2 mm) were fabricated with commercially pure titanium (grade 2) and were successively ground using grade 320 and 600 waterproof abrasive paper to remove the natural surface oxide. The samples were then ultrasonically cleaned in acetone, ethanol and distilled water. The titanium discs were subjected to a modified MAO treatment according to previous studies [8,27]. Anodizing was performed in an aqueous electrolyte at 400 V for 5 min by applying a d.c. field to the samples. The electrolyte contained 0.15 M calcium acetate monohydrate ($(CH_3COO)_2$-$Ca{\cdot}H_2O$, Wako, Japan) and 0.02 M calcium glycerophosphate ($C_3H_7CaO_6P$, Wako, Japan). All of the MAO processing was carried out in a water-cooled bath, with a stainless steel plate was used as the cathode. A magnetic stirrer was used to achieve homogeneity in the electrolyte and to eliminate air bubbles generated on the titanium surface during the process. After MAO treatment the samples were rinsed with distilled water and dried in an oven at 40 °C for 24 h. The samples were uniformly light gray.

In accordance with the electric polarization process reported in previous works [13–15] the MAO TiO_2 coated samples were sandwiched between a pair of platinum (Pt) plate electrodes, electrically polarized in a d.c. field of 5 kV cm^{-1} in air at 400 °C for 1 h and then cooled to room temperature under the applied d.c. voltage. The TiO_2 coating in contact with the anode was termed the negative surface (N surface), and the TiO_2 coating placed in contact with the cathode was called the positive surface (P surface). A non-polarized specimen was heated in air at 400 °C for 1 h under no field and termed the 0 surface.

The thermally stimulated depolarization current (TSDC) of the polarized samples were measured with a Hewlett–Packard 4140B pA meter. Each polarized sample was sandwiched between Pt electrodes and heated to 550 °C in an electric furnace equipped with a stainless steel shielded sample chamber at a heating rate of 5 °C min^{-1}. The total amount of stored charge was calculated as previously reported [17].

The surface morphologies and cross-sectional microstructures of the coatings before and after polarization were observed by scanning electron microscopy (SEM) (Hitachi S-3400NX, Tokyo, Japan). In addition, the elemental compositions and distributions of the coatings were also analyzed using energy-dispersive X-ray spectroscopy (EDX) in conjunction with the SEM system.

The phase compositions of the sample surfaces were analyzed by X-ray diffraction (XRD) (PW1700, PANalytical, Tokyo, Japan) in the 2θ range 10–70° using CuK_α radiation at 40 kV and 10 mA.

The chemical compositions of the sample surfaces were analyzed by X-ray photoelectron spectroscopy (XPS) (SSX-100, Surface Science Instruments, Mountain View, CA, USA) under ultrahigh vacuum. MgK_α (1253.6 eV) radiation was used as the X-ray source in the XPS tests. The XPS take-off angle was set to 90°. Charge effects were corrected using the C1s line of adventitious carbon at 285 eV. The XPS spectra were fitted using the Casa program to a Gaussian–Lorentzian peak shape with a Shirley baseline to represent the background. The composition of the coatings and thickness of the contaminant carbon layer were calculated according to methods used in a previous study [28].

The surface roughnesses of the samples were quantified using a laser profile micrometer (VF-7500, Keyence, Osaka, Japan) with a resolution of 0.01 μm. Six samples from each group were chosen at random and scanned. The scans were performed at three different positions on each sample. The R_a values are presented as means ± SD.

Contact angle measurements were performed using the sessile drop method at room temperature with a commercial contact angle meter (Kyowa Interface Measurement and Analysis System, Tokyo, Japan). Images were collected with a camera and the contact angle between the 1 μl droplet of deionized water and the coated surface was measured from the magnified image. Five samples from each group were used for contact angle measurement. The measurements were performed three times at different positions on each sample.

All values are presented as means ± SD, and commercial statistical software (Statcel, OMS Ltd, Saitama, Japan) was used for statistical analysis. One-way analysis of variance (ANOVA) was used following multiple comparisons with Scheffe's F-test to assess the data, and $P < 0.05$ was considered to indicate statistical significance.

3. Results and discussion

3.1. Structure and morphology of the MAO TiO_2 coatings

The surface morphology, cross-sectional microstructure, elemental compositions and distributions of the MAO TiO_2 coating are shown in Figs. 1 and 2. The figures show that a porous layer was formed on the surface of the Ti substrate after MAO treatment, with pore sizes of about 2–4 μm distributed homogeneously (Fig. 1a). These pits were optimized to produce an implant surface for interaction with bone [29]. The cross-section image reveals that the coating was approximately 10 μm thick (Fig. 1b). The EDX spectra demonstrate the presence of C, O, Ca, P and Ti (Fig. 2a). The Ca and P elements were incorporated and distributed homogeneously through the coating after MAO treatment (Fig. 2b). The Ca:P atomic ratio was 1.5.

The XRD patterns of the polarized and non-polarized MAO TiO_2 coatings are shown in Fig. 3. The MAO TiO_2 coating consisted of 32% rutile and 68% anatase. The phase content of TiO_2 was obtained using the Spurr equation [30]:

$$W_R = 1 - 1/(1 + 1.26(A_R/A_A)) \quad (1)$$

where W_R is the rutile content and A_A and A_R represent the diffraction intensities of anatase (101) and the rutile (110), respectively. The ratio between the rutile and anatase contents was controlled by the applied voltage [31]. Despite the existence of Ca and P in the electrolyte no Ca- or P-containing phases were detected by XRD [6]. The average MAO TiO_2 crystal size calculated from the (101) peak of anatase and the (110) peak of rutile was the same as that of pure TiO_2. There were no obvious changes in morphology or phase composition after electric polarization.

3.2. Spectroscopic investigation of the surface

XPS surveys of the MAO TIO_2 coatings were performed before and after electric polarization (Fig. 4a). The elements with the highest detected concentrations were Ti, O, C, Ca and P (Table 1). The atomic concentration (%) of each element in MAO TIO_2 was stable under polarization. The amount of organic contaminants, thickness 5 Å, in the surfaces also remained constant after polarization.

High resolution XPS spectra of O1s, Ca2p, P2p and $Ti2p_{3/2}$ were measured from the MAO coatings before and after electric polarization. The Ca2p spectra of the MAO surfaces reveal that the surface exhibits the typical double peak feature at 347.5 eV ($2p_{3/2}$) and 351.0 eV ($2p_{1/2}$) with a spin orbit splitting of 3.5 eV. This observation

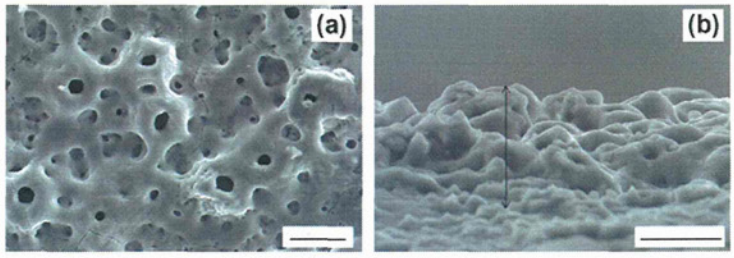

Fig. 1. SEM images of (a) a top view and (b) an oblique view (40°) of MAO TiO_2. An arrow indicates the coating range. The bar represents 10 μm.

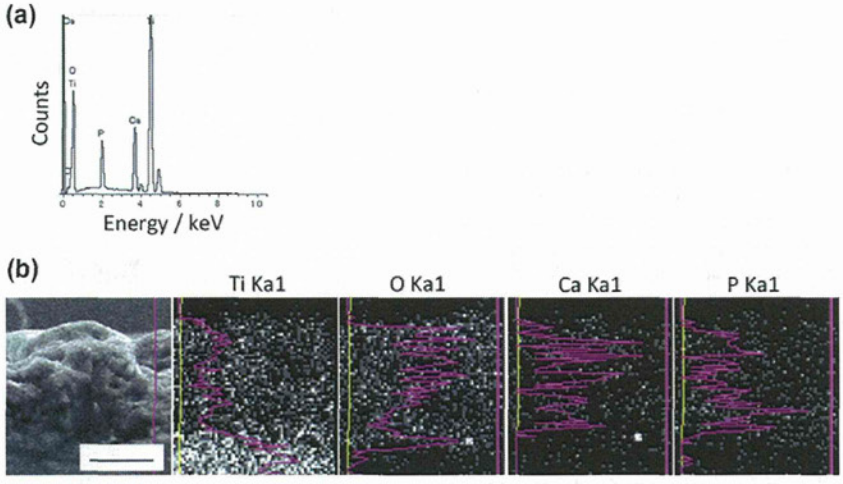

Fig. 2. EDX spectra of (a) a surface scan, (b) a line scan of a cross-section of the MAO TiO_2 coating. The bar represents 10 μm.

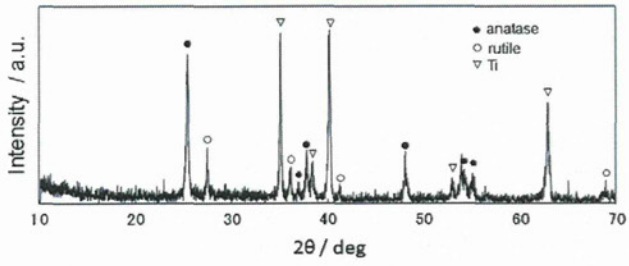

Fig. 3. XRD spectra of the MAO TiO_2 coating.

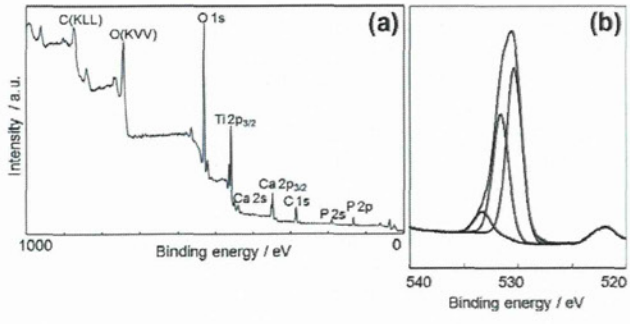

Fig. 4. Surveys of (a) the XPS spectra and (b) the O1s high resolution spectra of the non-polarized MAO TiO_2 coating.

provides evidence for divalent Ca-containing surface species [27]. The P2p spectra exhibited a single peak at 133.5 eV, suggesting that phosphorus exists in the samples in the pentavalent oxidation state

Table 1
Elemental composition detected by XPS.

Sample	Elemental composition (at.%)			
	O	Ti	Ca	P
0 surface	73	14	7	6
P surface	73	15	7	5
N surface	73	15	7	5

(P^{5+}) [27]. Ti–P bonds were not observed in the samples because the characteristic peak of P in Ti–P at 129 eV was not present in the spectra. No discernible changes were observed in the peak positions or full widths at half maximum (FWHM) of the Ca2p and P2p spectra after polarization. The $Ti2p_{3/2}$ spectrum was resolved into three spin orbit components according to the oxidation states at binding energies (BE) of 455.2, 457.0 and 459.1 eV, which represent the TiO, Ti_2O_3 and TiO_2 fractions in the samples, respectively [32]. The intensities of the deconvoluted components show that the dominant surface state is Ti^{4+} on all surfaces, and the intensity ratios of Ti^{4+} of the samples are all the same. This result indicates that polarization has little effect on the Ti state of MAO TiO_2 coatings. The O1s spectra were deconvoluted into three kinds of oxygen bonds at BE of 530.5, 531.7 and 533.5 eV, which represent oxide species (O^{2-}), dissociative water (hydroxyl groups)/phosphate groups (OH^- or PO_4^{3-}) and adsorped molecular water (H_2O), respectively (Fig. 4b) [33,34]. The area ratios of the three peaks in the O1s spectra of the different surfaces are listed in Table 2. The intensities of the H_2O spectra from the polarized specimens were enhanced compared with those of the non-polarized samples. The largest surface OH groups/O^{2-} ratio of 54% was found at the P surface, followed by 53% at the 0 surface and 44% at the N surface. This result suggests that the P surface

Table 2
Percentage areas of the deconvoluted peaks in the O1s XPS spectra.

Sample	Percentage area		
	530.5 eV	531.7 eV	533.5 eV
0 surface	60	32	7.4
P surface	59	32	8.0
N surface	63	28	8.1

was the most reduced of all of the specimens, while the N surface retained an oxidizing state. There were oxygen and oxygen vacancy distribution gradients in the three samples.

3.3. TSDC spectrum and stored electric charge

The behavior of a polarized material can be estimated by TSDC measurements. TSDC analysis is a widely used experimental technique to investigate the qualities of polarized materials such as stored charges, activation energies for depolarization processes and relaxation times. Ionic polarization inside a material causes the generation of TSDC when the material temperature is increased. Representative TSDC spectra of the non-polarized and polarized MAO TiO_2 samples are shown in Fig. 5. The TSDC curve begins to increase at ca. 200 °C, reaches a maximum at ca. 500 °C, and then gradually decreases. The average stored charges of the non-polarized specimen and the polarized samples calculated from the TSDC curves were 2.6 and 21 μC cm^{-2}, respectively. This result confirms that MAO TiO_2 coatings can be polarized under the experimental conditions utilized. These results also confirm that the polarized specimens maintain the same surface polarization state after 3 months. The activation energy for depolarization of MAO TiO_2 was 0.85 eV, calculated from the TSDC spectrum. The activation energy observed was close to the values of activation energy for conductivity reported for nanoporous TiO_2 films [35]. The result suggests that the charge carriers in electrical conduction of nanoporous TiO_2 films also play a role in the polarization of MAO TiO_2. The process underlying the polarization treatment can be explained as follows. Ti^{2+} and Ti^{3+} exist in MAO TiO_2, as shown in the XPS analysis, and oxygen vacancies (Vö) are present in the coating. Vö accumulate on the cathodic side (P surfaces) but are depleted on the anodic side (N surfaces) under a d.c. field and at elevated temperatures because Vö occur in TiO_2 ceramics [36]. Thus a Vö concentration gradient is produced. Oxygen and Vö should play essential roles in the electric polarization of TiO_2 under a d.c. field.

The samples enter a metastable state when they are cooled to room temperature and the d.c. field is removed. On the other hand, when the temperature is elevated in air, a slight reduction of the TiO_2 surface occurs, described by the reaction:

$$2O_O^{\times} \leftrightarrow 2V\ddot{o} + 4e' + O_2(g) \quad (2)$$

The electrons produced by this reaction cause currents in non-polarized TiO_2. That is to say, there are at least two polarization pathways responsible for the TSDC of the polarization samples. The currents responsible for space charge polarization remain after subtraction of the reduction currents.

3.4. Water contact angle on the surface

Fig. 6 shows the results of static water contact angle measurements on the MAO TiO_2 surfaces after heating only or after electric polarization. The initial water contact angle on the untreated surface was 73.1 ± 4.2°, which decreased to below 10° after heating or polarization. Four days later the water contact angle of the non-polarized surface returned to 62.5 ± 9.7°, but was 27.4 ± 11.4° on the P surface and 10.3 ± 2.1° on the N surface. One month later

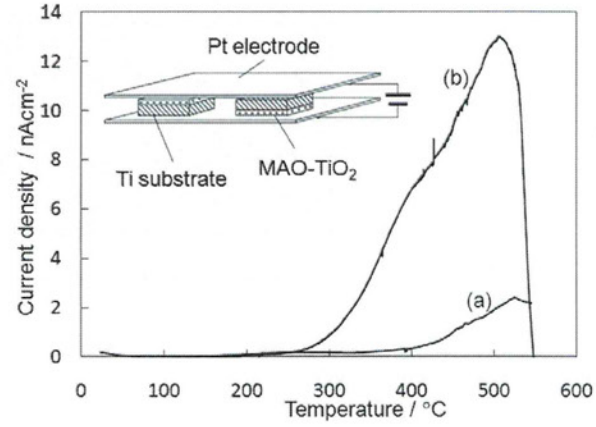

Fig. 5. Thermally stimulated depolarization current (TSDC) spectra of (a) non-polarized and (b) polarized MAO TiO_2 coatings and schematics of the polarization system.

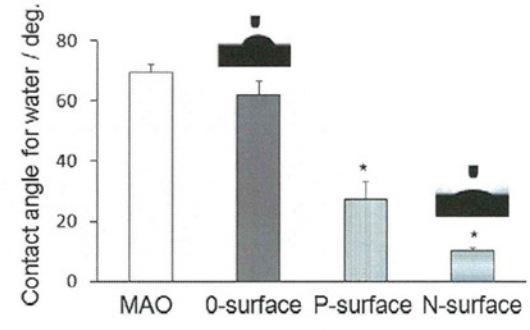

Fig. 6. Water contact angle measurements of the MAO TiO_2 coating and the 0 surface, N surface and P surface 4 days after heat or polarization treatment. Side view images of 1 μl of water dropped onto the 0 surface and N surface are also presented.

the water contact angle returned to 41.8 ± 3.1° on the P surface and 48.7 ± 5.5° on the N surface. Surface reduction mediated by the heat treatment may return over time due to the adsorption of oxygen or water from the air. In contrast, the electrically polarized MAO TiO_2 maintained its surface hydrophilicity. The surface roughnesses (R_a values) of the 0 surface, N surface and P surface are 1.2 ± 0.042, 1.2 ± 0.015 and 1.2 ± 0.035 μm, respectively, suggesting that polarization does not alter the surface roughness.

The MAO TiO_2 surface is subject to oxygen loss under thermal reduction conditions, and accordingly surface Vö are created. Water adsorption onto the TiO_2 surface is described by either a molecular or a dissociative mechanism. Dissociative water at oxygen vacancies results in two bridging OH groups for each vacancy site [37]. One of these OH groups can be thought of as comprising oxygen from the water molecule adsorbed at the vacancy, while the second results from hydrogen transfer to a neighboring bridging oxygen anion site. In principle these two bridging OH groups are indistinguishable. These surface OH groups result in superhydrophilicity at the surfaces immediately after heat treatment. The H_2O–TiO_2 interactions observed on thermal activation at oxygen vacancy sites are similar to interactions under UV illumination in that Ti^{3+} sites were formed [38,39]. However, it has been reported that reversible oxidation occurs in crystalline TiO_2 samples with thermal defects heated to high temperatures in air, and that the oxygen defects are rapidly compensated for [32]. This process causes the hydrophilicity of the 0 surface to change within several days. This result also suggests that high temperature treatment

promotes the mobility of oxygen and Vö in the TiO_2 oxide lattice. The movement of oxygen and Vö can produce a gradient of charges in polarized MAO TiO_2. Although the surface OH groups on the Ti surface and the removal of adsorbed organic contaminants are assumed to play important roles in photoinduced hydrophilicity [40,41], other factors such as hydration forces have also recently been studied [42,43]. In this study the wettability of the polarized samples was not correlated with the number of surface OH and absorbed organic species. One factor that produced a lasting reduction in the water contact angle might be the electrowetting effect. The electrowetting effect can be defined as a change in the solid–liquid contact angle due to an electric field applied to the solid and the liquid [44]. The forces that result from the applied electric field tend to pull the droplet down onto the electrode, lowering the macroscopic contact angle and increasing the droplet contact area [45]. The electric polarization treatment in this experiment resulted in the formation of a capacitor at the interface between the TiO_2 surfaces and deionized water, partially dissociated into H_3O^+ and OH^- at room temperature. The electrostatic forces decrease the surface energy and the contact angle. Because there were equal quantities of stored electric charges on the N surface and the P surface the enduring reduction in contact angle was nearly the same on both surfaces [19,20]. Similar results have also been observed in other research where both positive and negative surfaces showed symmetrical electrowetting [46,47].

4. Conclusions

The experimental results demonstrated that MAO TiO_2 coatings are polarizable materials, similar to previous reports regarding other bioceramics. The metastable state produced by the electric fields induced surface charges on both surfaces, termed the N surface and the P surface. The polarized MAO TiO_2 surfaces do not exhibit any obvious changes in morphology, surface roughness or phase components in SEM, EDX and XRD observations. However, the electric polarization treatment resulted in changes to the surface chemical composition and the surface wettability. XPS analysis revealed that the oxygen binding energies of the three surfaces were different, and several days after the procedure the polarized surfaces became more hydrophilic than the non-polarized surface due to the induced surface charges. The polarized MAO TiO_2 has good geometry and lasting wettability, suggesting potential uses in the surface modification of Ti implants.

Acknowledgements

This work was supported by the Nippon Foundation–Sasakawa Memorial Health Foundation Program, Japan, and Grants-in-Aid for Scientific Research (C) (20500405) from the Japan Society for the Promotion of Science.

Appendix A. Figures with essential colour discrimination

Certain figures in this article, particularly Figure 2, are difficult to interpret in black and white. The full colour images can be found in the on-line version, at doi:10.1016/j.actbio.2011.09.021.

References

[1] Brunette DM, Tengvall P, Textor M, Thomsen P. Titanium in medicine: material science, surface science, engineering, biological response and medical applications. Berlin: Springer Verlag; 2001.
[2] Long M, Rack HJ. Titanium alloy in total joint replacement – a materials science perspective. Biomaterials 1998;19:1621–39.
[3] Li J, Hastings GW. Oxide ceramics: inert ceramic materials in medicine and dentistry. In: Black J, Hastings G, editors. Handbook of biomaterial properties. London: Chapman & Hall; 1998. p. 340–54.
[4] Liu XY, Paul KC, Ding CX. Surface modification of titanium, titanium alloys, and related materials for biomedical applications. Mater Sci Eng R 2004;47:49–121.
[5] Junker R, Dimakis A, Thoneick M, Jansen JA. Effects of implant surface coatings and composition on bone integration: a systematic review. Clin Oral Implants Res 2009;20:185–206.
[6] Ishizawa H, Ogino M. Formation and characterization of anodic titanium oxide films containing Ca and P. J Biomed Mater Res 1995;29:65–72.
[7] Yerokhin AL, Nie X, Leyland A, Matthews A, Dowey SJ. Plasma electrolysis for surface engineering. Surf Coat Technol 1999;122:73–93.
[8] Han Y, Xu KW. Photoexcited formation of bone apatite-like coatings on micro-arc oxidized titanium. J Biomed Mater Res A 2004;71:608–14.
[9] Frauchiger VM, Schlotting F, Gasser B, Textor M. Anodic plasma-chemical treatment of CP titanium surfaces for biomedical applications. Biomaterials 2004;25:593–606.
[10] Sul YT, Johansson CB, Petronis S, Krozer A, Jeong Y, Wennerberg A, et al. Characteristics of the surface oxides on turned and electrochemically oxidized pure titanium implants up to dielectric breakdown: the oxide thickness, micropore configurations, surface roughness, crystal structure and chemical composition. Biomaterials 2002;23:491–501.
[11] Sul YT. The significance of the surface properties of oxidized titanium to the bone response: special emphasis on potential biochemical bonding of oxidized titanium implant. Biomaterials 2003;24:3893–907.
[12] Giavaresi G, Fini M, Cigada A, Chiesa R, Rondelli G, Rimondini L, et al. Mechanical and histomorphometric evaluations of titanium implants with different surface treatments inserted in sheep cortical bone. Biomaterials 2003;24:1583–94.
[13] Yamashita K, Kitagaki K, Umegaki T. Thermal instability and proton conductivity of ceramic hydroxyapatite at high temperatures. J Am Ceram Soc 1995;78:1191–7.
[14] Wang W, Itoh S, Yamamoto N, Nagai A, Yamashita K. Electrical polarization of β-tricalcium phosphate ceramics. J Am Ceram Soc 2010;93:2175–7.
[15] Tanaka K, Nakamura S, Yoshida K, Hashimoto K, Toda Y, Yamashita K. Effects of electrical polarization on B-type carbonated hydroxyapatite. Phos Res Bull 2004;17:126–9.
[16] Kobayashi M, Saito H, Mase T, Sasaki T, Wang W, Tanaka Y, et al. Polarization of hybridized calcium phosphoaluminosilicates with 45S5-type bioglasses. Biomed Mater 2010;5:25001.
[17] Ueshima M, Nakamura S, Yamashita K. Huge-millicoulomb charge storage in ceramic hydroxyapatite by bimodal electric polarization. Adv Mater 2002;14:5915–7.
[18] Tarafder S, Banerjee S, Bandyopadhyay A, Bose S. Electrically polarized biphasic calcium phosphates: adsorption and release of bovine serum albumin. Langmuir Lett 2010;26:16625–9.
[19] Nakamura M, Nagai A, Hentunen T, Salonen J, Sekijima Y, Okura T, et al. Surface electric fields increase osteoblast adhesion through improved wettability on hydroxyapatite electra. ACS Appl Mater Interfaces 2009;1:2181–9.
[20] Bodhak S, Bose S, Bandyopadhyay A. Role of surface charge and wettability on early stage mineralization and bone cell–materials interactions of polarized hydroxyapatite. Acta Biomater 2009;5:2178–88.
[21] Itoh S, Nakamura S, Nakamura M, Shinomiya K, Yamashita K. Enhanced bone ingrowth into hydroxyapatite with interconnected pores by electrical polarization. Biomaterials 2006;27:5572–9.
[22] Kobayashi T, Itoh S, Nakamura S, Nakamura M, Shinomiya K, Yamashita K. Enhanced bone bonding of hydroxyapatite-coated titanium implants by electrical polarization. J Biomed Mater Res A 2007;82:145–51.
[23] Ruardy TG, Schakenraad JM, van der Mei HC, Busscher HJ. Adhesion and spreading of human skin fibroblasts on physiochemically characterized gradient surfaces. J Biomed Mater Res 1995;29:1415–23.
[24] Liao HH, Andersson AS, Sutherland D, Petronis S, Kasemi B, Thomsen P. Response of rat osteoblast-like cells to microstructured model surfaces in vitro. Biomaterials 2003;24:649–54.
[25] Yang B, Uchida M, Kim HM, Zhang XD, Kokubo T. Preparation of bioactive titanium metal via anodic oxidation treatment. Biomaterials 2004;25:1003–10.
[26] Wei DQ, Zhou Y, Jia DC, Wang YM. Characteristic and in vitro bioactivity of a microarc-oxidized TiO_2-based coating after chemical treatment. Acta Biomater 2007;3:817–27.
[27] Song WH, Jun YK, Han Y, Hong SH. Biomimetic apatite coatings on microarc oxidized titania. Biomaterials 2004;25:3341–9.
[28] Hanawa T, Kamiura Y, Yamamoto S, Kohgo T, Amemiya A, Ukai H, et al. Early bone formation around calcium-ion-implanted titanium inserted into rat tibia. J Biomed Mater Res 1996;36:131–6.
[29] Hansson S, Norton M. The relation between surface roughness and interfacial shear strength for bone-anchored implants. A mathematical model. J Biomech. 1999;32:829–36.
[30] Spurr RA, Myers H. Quantitative analysis of anatase–rutile mixture with an X-ray diffractometer. Anal Chem 1957;29:760–2.
[31] Huang P, Wang F, Xu K, Han Y. Mechanical properties of titania prepared by plasma electrolytic oxidation at different voltages. Surf Coat Technol 2007;201:5168–71.
[32] Lu G, Bernasek SL, Schwartz J. Oxidation of a polycrystalline titanium surface by oxygen and water. Surf Sci 2000;458:80–90.
[33] Hugenschmidt MB, Gamble L, Campbell CT. The interaction of H_2O with a TiO_2 (110) surface. Surf Sci 1994;302:329–40.
[34] Wang LQ, Baer DR, Engelhard MH, Shultz AN. The adsorption of liquid and vapor water on TiO_2 (110) surfaces: the role of defect. Surf Sci 1995;344:237–50.

[35] Dittrich Th, Weidmann J, Koch F, Uhlendorf I, Lauemann I. Temperature- and oxygen partial pressure-dependent electrical conductivity in nanoporous rutile and anatase. Appl Phys Lett 1999;75:3980–2.
[36] Sheng J, Fukami T, Karasawa J. X-ray photoemission spectroscopy (XPS) and thermally stimulated current (TSC) studies on the resistance degradation of iron-doped titania ceramics. J Am Ceram Soc 1998;81:260–2.
[37] Perron H, Vandenborre J, Domain C, Drot R, Roques J, Simoni E, et al. Combined investigation of water sorption on TiO_2 rutile (110) single crystal face. XPS vs. periodic DFT. Surf Sci 2007;601:518–27.
[38] Henderson MA, Epling WS, Peden CHF, Perkins CL. Insights into photoexcited electron scavenging processes on TiO_2 obtained from studies of the reaction of O_2 with OH groups adsorbed at electronic defects on TiO_2(110). J Phys Chem B 2003;107:534–45.
[39] Diebold U. The surface science of titanium dioxide. Surf Sci Rep 2003;48:53–229.
[40] Sakai N, Fujishima A, Watanabe T, Hashimoto K. Quantitative evaluation of the photoinduced conversion properties of TiO_2 thin film surfaces by the reciprocal of contact angle. J Phys Chem B 2003;107:1028–35.
[41] Mills A, Crow M. A study of factors that change the wettability of titania films. Int J Photoenergy 2008;470670.
[42] Jribi R, Barthel E, Bluhm H, Grunze M, Koelsch P, Verreault D, et al. Ultraviolet irradiation suppresses adhesion on TiO_2. J Phys Chem C 2009;113:8273–7.
[43] Takahashi K, Yui H. Analysis of surface OH groups on TiO_2 single crystal with polarization modulation infrared external reflection spectroscopy. J Phys Chem C 2009;113:20322–7.
[44] Mugele F, Baret JC. Electrowetting: from basics to applications. J Phys Condens Mater 2005;17:R705–74.
[45] Fan SK, Yang H, Wang TT, Hsu W. Asymmetric electrowetting moving droplets by a square wave. Lab Chip 2007;7:1330–5.
[46] Vallet M, Vallade M, Berge B. Limiting phenomena for the spreading of water on polymer films by electrowetting. Eur Phys J 1999;11:583–91.
[47] Raj B, Dhindsa M, Smith NR, Laughin R, Heikenfeld J. Ion and liquid dependent dielectric failure in electrowetting systems. Langmuir 2009;25:12387–92.

Bull. Mater. Sci., Vol. 34, No. 7, December 2011, pp. 1289–1296. © Indian Academy of Sciences.

Preparation of novel polymer–metal oxide nanocomposites with nanophase separated hierarchical structure

K NAM[1,2], Y TSUTSUMI[1], C YOSHIKAWA[3], Y TANAKA[1], R FUKAYA[1], T KIMURA[1,2], H KOBAYASHI[4], T HANAWA[1,*] and A KISHIDA[1,2,*]

[1]Institute of Biomaterials and Bioengineering, Tokyo Medical and Dental University, 2-3-10 Kanda-Surugadai, Chiyoda-ku, Tokyo 101-0062, Japan
[2]Japan Science and Technology Agency, CREST 5, Sanbancho, Chiyoda-ku, Tokyo 102-0075, Japan
[3]International Centre for Materials Nanoarchitectonics (MANA), National Institute for Materials Science (NIMS), Tsukuba, Ibaraki 305-0044, Japan
[4]Biomaterials Centre, National Institute for Materials Science (NIMS), Tsukuba, Ibaraki 305-0044, Japan

MS received 7 April 2010; revised 16 January 2011

Abstract. This article deals with preparation of nanocomposite which comprised of nanophase separated structure of polymer chains and metal oxide. By grafting poly(hydroxyethyl methacrylate), poly(HEMA) on the surface of titanium which is covered by passive titanium oxide by atom transfer radical polymerization (ATRP) and executing anodic polarization, hierarchy nanophase separated structure with controlled thickness can be obtained. The titanium ions would be cationically charged and completely filled up the unoccupied binding sites of the polymer chains via electrochemical reaction, eventually covering the polymer chains with titanium oxide. However, this structure can be obtained when the anodic polarization is executed at initial applied voltage exceeding 10 V_{SCE}. The control of thickness is possible by controlling the initial applied voltage. These results prove that the conventional polymer can form composite structure with metal oxide without using fillers or special polymers designed for composite.

Keywords. Atom transfer radical polymerization; anodic polarization; nanocomposite.

1. Introduction

The main purpose of the preparation of the nanocomposite is to obtain the synergic effect of the polymer and the inorganic compound. Nanocomposites have a peculiar structure, i.e. a phase separated structure, with a nanoscale interface between the polymer matrix and the inorganic compound (nanophase separated structure). This phase separated structure plays a very important role in the production of a molecular-level synergic effect between the organic and inorganic compounds in nanocomposites (Paul and Robeson 2008). In general, nanocomposites with a phase separated structure in nanoscale can be prepared by four different methods: (i) embedding an inorganic moiety into the polymer, (ii) using interpenetrating polymer networks with chemical bonds, (iii) incorporating inorganic groups by bonding them to the polymer backbone and (iv) forming a dual inorganic–organic hybrid polymer (Kickelbick 2003). These structures can be created by a sol–gel process, core-shell composite, the electrodeposition of conductive polymers such as polyaniline, exfoliated claybased nanocomposite, and the self-assembly or assembly of nano building blocks for the formation of mesophase structures (Sudheendra and Raju 1999; Sanchez *et al* 2001; Kickelbick 2003; Lahav *et al* 2006; Angelomé *et al* 2005; Ivanovici *et al* 2008).

Nanocomposites with nanophase separated structures prepared by conventional methods have a common feature. The type of polymers that can be used for their preparation is limited to organic metals such as polyaniline or organo-functional metal alkoxides (Wessling 1997; Kickelbick 2003). This is because the affinity between organic and inorganic molecules is low, and the modification of physical property may allow the preparation of nanocomposites using only polymers and metal oxides. So, the selection of the polymer for the composite preparation is limited. Additionally, a polymer matrix exists as a gel phase or a polymer aggregate. Hence, it is very important to homogenously disperse the metal oxide throughout the polymer matrix in order to form a homogeneous nanophase separated structure. Alternative method for the creation of the nanocomposite without using organic metals is to apply the nanofiller such as nanoparticles or nanotubes to produce exfoliated clay-based nanocomposite. This method is good in the fact that conventional polymer can be used for the nanocom-

*Author for correspondence
(hanawa.met@tmd.ac.jp; kishida.fm@tmd.ac.jp)

posite production and reinforcement of the mechanical strength, but possesses poor miscibility, dispersion and interfacial strength (Yang *et al* 2006; Xu *et al* 2008).

This paper describes a method for preparation of polymer–metal oxide nanocomposites with a nanophase separated structure, using conventional polymer such as poly (hydroxyethyl methacrylate) and metal oxide such as titanium oxide without using inorganic nanofillers or organic metals to construct electrode for biosensor. In order to prepare polymer–metal oxide nanocomposites with a nanophase separated structure, the homogeneous dispersion of metal ions, an increase in the concentration of the metal oxide, and a reduction in the size of the polymer–metal ion oxide interface are very important since they essentially alter the physical property of the nanocomposite. The most appropriate way would be to construct a hierarchical structure of polymer and metal oxide. It may be possible to achieve homogeneous metal oxide distribution with a high concentration by creating a layer of metal oxide between the polymer chains consisting of monolithic and continuous phase of metal oxide structure. The interface of polymer and metal oxide can be reduced to nanoscale when the polymer layer is a simple stretched polymer chain with uniaxial orientation. The monolithic and continuous phase of metal oxide structure which may function as the route for the electrons is required between non-electroconductive polymers to create a hetero-electroconductive surface.

Several requirements should be carefully considered in order to obtain such structures: a stretched polymer chain with a uniaxial orientation should be prepared, the problem of affinity between polymers and metal oxides should be solved and the metal oxide should be placed appropriately between the polymer chains. We attempted to control the rotational movement and uniaxial orientation of polymer chains by grafting them, i.e. by grafting a so called polymer brush on the surface of a substrate. This method is useful for completely suppressing the movement of one chain terminal; various polymers can thus be adopted. However, if the density of the grafted polymer chains is < 0.0065 chains/nm^2, the chain will collapse, leading to the adsorption of the polymer onto the surface of the substrate (Tsujii *et al* 2006). Moreover, height of the grafted polymer chains should be equal; otherwise, blobs may be formed among the chains (de Gennes *et al* 1980).

Atom transfer radical polymerization (ATRP) via surface initiation can solve this problem. This method is useful since a high density polymer brush with a uniform chain length and fully extended chain conformation can be prepared (Tsujii *et al* 2006; Yoshikawa *et al* 2006). For the preparation of metal oxides, we carried out anodic polarization of titanium; this technique is beneficial because it is simple and height of the metal oxide layer formed on the surface of the substrate can be controlled by controlling the applied voltage (Weatherall 1992). Since titanium is covered with passive titanium oxide where the composition is mainly TiO_2, when the titanium surface is treated with anodic polarization, TiO_2 is expected to grow between the unoccupied binding sites of the polymer brush by electrochemical reaction; it would thus be possible to create a 'metal oxide mesh' in the polymer brush (figure 1). Using this, we prepared a polymer–metal oxide nanocomposite with a nanophase separated hierarchical structure by grafting a polymer brush on the surface of a titanium substrate and carrying out anodic polarization.

2. Experimental

2.1 *Grafting high density polymer brush on titanium surface*

A titanium plate was mirror-polished with SiC paper and SiO_2 suspension. The plates were ultrasonically washed in acetone and ethyl alcohol for 15 min each. The surface of the titanium plate was characterized by XPS, and it showed normal surface characteristics. The titanium substrate was covered with a TiO_2 layer having a thickness of a few nanometers.

Hydroxyethyl methacrylate (HEMA) was purified under the conditions proposed by Beers *et al* (1999), and it was sealed and refrigerated. 6-(2-bromo-2-isobutyloxy)-hexyltriethoxysilane (BHE) was synthesized according to the method reported by Ohno *et al* (Beers *et al* 1999; Ohno *et al* 2005). Cu(I)Br, bipyridine and ethyl 2-bromoisobutylate (EBIB) were purchased and used without further purification. All the solvents used in this study were dehydrated before use. The modification of the titanium surface with the initiator was carried out by silane coupling (Ohno *et al* 2005; Yoshikawa *et al* 2006). The titanium substrate was immersed in a tetrahydrofuran solution of ammonium water (1 wt%) and BHE (1 wt%) for 12 h at room temperature to chemically deposit BHE on its surface. Subsequently, the titanium surface with BHE was rinsed with THF and methanol to obtain a BHE initiated titanium substrate.

Cu(I)Br (25 mM) and bipyridine (63 mM) were mixed in methanol for ~30 min to solubilize Cu(I)Br completely. A mixture of HEMA (4·5 M) and free initiator EBIB (22·5 mM) was added to the methanol solution and mixed for a short period of time. A certain amount of this solution was then poured into a glass tube in which the BHE initiated titanium substrate was placed. The tube was sealed tightly and placed in a shaking water bath. Polymerization was carried out for 90 min at 40°C. After polymerization, the polymer solution was diluted in dimethylformaldehyde (DMF) solution for performing gel permeation chromatography (GPC) (CCP&8020-series high-speed liquid chromatograph, Tosoh, Japan) measurements equipped with two Shodex gel column LF804